Understanding the Synergistic Effect of Device Architecture Design toward Efficient Perovskite Light-Emitting Diodes Using Interfacial Layer Engineering

Eojin Yoon, Kyung Yeon Jang, Jinwoo Park, and Tae-Woo Lee*

Metal halide perovskite (MHP) light-emitting diodes (LEDs) have been widely studied and have been reached to >20% external quantum efficiency, owing to their attractive characteristics (e.g., solution processability, tunable bandgap and extremely high color purity, high mobility). During the rapid development of perovskite light-emitting diodes (PeLEDs), modifying the device architecture has been widely studied as well as improving the crystal quality of MHP to achieve near-unity photoluminescence quantum yield. However, efforts in device architecture engineering have received less attention despite their significance. Here, strategies are reviewed to enhance the efficiency of PeLEDs in terms of the device engineering by interfacial charge injection/transport, exciton-quenching blocking, and defect passivation layers for enhancing radiative electron–hole recombination. Strategies are systematically classified for each layer in PeLEDs and discussed the synergetic effect between different strategies. Perspective is also provided on future research on PeLEDs focusing on their architecture.

1. Introduction

Metal halide perovskite (MHPs) are ionic crystal with the chemical formula of ABX_3, where A is monovalent cation (e.g., methylammonium (MA^+), formamidinium (FA^+), and Cs^+), B is divalent metal cation (e.g., Pb^{2+}, Sn^{2+}) and X is halide anion (Cl^-, Br^-, I^-). MHP has gained great attention due to their superior electrical and optical properties and showed high potential for various optoelectronic application including solar cells,[1,2] lasers,[3,4] photodetectors,[5,6] and light-emitting diodes (LEDs).[7–11]

E. Yoon, K. Y. Jang, J. Park, Prof. T.-W. Lee
Department of Materials Science and Engineering
Seoul National University
1 Gwanak-ro, Gwanak-gu, Seoul 08826, Republic of Korea
E-mail: twlees@snu.ac.kr
Prof. T.-W. Lee
School of Chemical and Biological Engineering
Seoul National University (SNU)
1 Gwanak-ro, Gwanak-gu, Seoul 08826, Republic of Korea
Prof. T.-W. Lee
Institute of Engineering Research
Research Institute of Advanced Materials
Nano Systems Institute (NSI)
Seoul National University
1 Gwanak-ro, Gwanak-gu, Seoul 08826, Republic of Korea

The ORCID identification number(s) for the author(s) of this article can be found under https://doi.org/10.1002/admi.202001712.

MHP is tolerant of defects; most of the point defects in MHP located near the band edge.[12,13] Therefore, even many point defects can be generated during the crystallization of MHP, they do not critically degrade the performance of the optoelectronic devices.[12,13] Typically for LED application, defect tolerant nature of MHP can enable the emission layer with high photoluminescence quantum yield (PLQY > 90%) and high color purity (full-width half maximum (FWHM) ≈ 20 nm)). Unlike traditional colloidal quantum dots (cQDs), their high color purity is rarely affected by the size distribution of their crystal or particles when their size is over exciton Bohr diameter (beyond quantum confinement regime).[14,15]

The X-site halide anion strongly affects the bandgap of the MHP.[16–18] Reduction in the size of the halide anion increases the band gap because of increased orbital interaction between Pb 6s and halide anion np (n = 3, 4, 5).[19] Therefore, the emission wavelength of MHP can be easily tuned by controlling the composition of halide anion. Owing to their defect tolerant nature and facile color tunability, perovskite light-emitting diodes (PeLEDs) gained great attention for high potential for realizing the next generation display which fulfills Rec. 2100 standard (red ≈ 630 nm, green ≈ 530 nm, and blue ≈ 465 nm). Consequently, their external quantum efficiency (EQE) for infrared, red- and green-emitting LEDs has been increased to >20%, which is comparable to those of conventional LEDs that use organic emitters or cQDs.[11,20–25] The EQE of blue-emitting PeLEDs has also been increased to >10%.[11]

There are two major subfields in PeLED research; i) nanoparticle (NP) which exploit colloidal synthesis and ii) polycrystalline (PC) where MHP directly crystallized on the substrate. For both subfields, the key strategies to achieve high-efficiency PeLED is to confine excitons in small grain or NP.[10,26] MHP have intrinsically low exciton binding energy, thus the generated exciton can easily dissociate into free carriers and reduce the PLQY.[10] In a reduced size of grain or NP, exciton can be spatially confined to limit the exciton diffusion length and facilitate the radiative recombination. Typically, for PC MHP, the addition of volatile nonsolvent while the crystallization process of MHP (nanocrystal pinning, NCP) can significantly reduce the grain size.[10] NCP process usually exploits highly volatile nonpolar solvent (e.g., chloroform) to induce fast crystallization.[10,27] In the NCP process, an organic

ADVANCED
SCIENCE NEWS
www.advancedsciencenews.com

ADVANCED
MATERIALS
INTERFACES
www.advmatinterfaces.de

solution, in which small amount of organic small molecule is added to the nonsolvent as an additive, can be applied on the quasi-MHP film during spinning to further reduce the grain size.[10,27,28] Spatial confinement of exciton can also be achieved by reducing the dimension of MHP. Typically, quasi-2D MHP using large ammonium bromide (e.g., phenylethyl-ammonium bromide)[29,30] and 0D MHP NP using organic ligands[31–34] have been widely studied.

In PC MHP without sufficient confinement, the bimolecular recombination of free carriers is dominant and PL lifetime accordingly decreases with increasing carrier density.[26,35] Slow bimolecular dominant recombination competes with nonradiative trap-related recombination.[35,36] Therefore, PLQY can be significantly reduced at the low charge-carrier density and with increasing trap density. On the other hand, confined MHP crystal (e.g., quasi-2D MHP, 0D MHP NP) have dominant excitonic recombination with significantly shorter PL lifetime compared to PC MHP.[26,35]

Regardless of the dimension of MHP, at high charge carrier density $>10^{17}$ cm^{-3}, trimolecular Auger recombination becomes dominant over excitonic or bimolecular radiative recombination and thus PLQY rapidly decrease.[26,36,37] Auger recombination in MHP at high carrier density is related to the efficiency roll-off in PeLEDs, which will be discussed further in the following chapters.[36]

To boost the efficiency of PeLEDs, device architecture designing should be considered simultaneously to carrier recombination in MHP crystal. PeLED typically consists of various layers including anode, hole injection layer (HIL), hole transport layer (HTL), emitting layer (EML), electron transport layer (ETL), electron-injection layer (EIL), and cathode. Each of these layers should be optimized considering various factors (e.g., thickness, mobility, band alignment) because they can synergistically affect PeLED efficiency. An LED converts electronic energy to light; the conversion efficiency is called EQE, which is the ratio of the number of photons emitted out of the device to the number of injected electrons.[38] EQE is strongly affected by the architecture of the device, so fabrication of highly efficient PeLEDs requires an understanding of this relationship. EQE is the product of four parameters:

$$EQE = \gamma \times \eta_{rad,eff} \times \eta_{S/T} \times \eta_{out} \tag{1}$$

γ is the electrical efficiency; it quantifies the proportion of injected carriers that are converted to excitons; γ can be maximized by balancing the supplies of holes and electrons in the EML to effectively create excitons from injected charges. $\eta_{rad,eff}$ represents the effectiveness of radiative recombination, and can be increased by blocking non-radiative recombination paths that form as a result of defects or luminescence quenching centers. $\eta_{S/T}$ represents the creation fraction of photons of the generated excitons in the EML. η_{out} is the outcoupling efficiency; it is high if photons generated in the EML easily escape from the device; the device structure strongly affects this factor. In short, highly efficient LEDs require well-balanced charge injection, dominant radiative recombination, and expeditious light outcoupling. Those factors have been successfully controlled by engineering the device architecture. The most distinct features in PeLEDs that are different from organic LEDs (OLEDs) is

facile luminescence quenching at the interfaces adjacent to the EML which stems from low exciton binding energy and long exciton diffusion length in MHPs.[10]

Typically for PeLED, device architecture should be more delicately controlled. Mobility of MHP is several orders higher than those of conventional EML (organic small molecule, polymer, and cQD), injected charges quickly traverse through EML. Therefore, serious charge imbalance can be caused to reduce the efficiency and excess charges can easily accumulate at the interface between MHP and neighboring layers.[39–42] Accumulated charges in EML can degrade MHP.[39–42] Also, accumulated charges can easily migrate to the counterpart transport layer (holes to ETL, electrons to HTL), due to relatively deep highest occupied molecular orbital (HOMO) level of MHP compared to conventional organic emitters. Leakage of major carrier reduces the efficiency and induce unwanted emission from the transport layer.[43] Deep HOMO level of MHP is also related to inefficient hole injection; HIL or HTL in PeLED should provide a deeper HOMO level than in conventional OLED for efficient hole injection and transport.[9]

Due to their long exciton diffusion length, MHP is critically affected by the interfaces. Reducing the nonradiative recombination site (e.g., diffused metal cation) and passivating the defects using an interfacial layer can significantly enhance the efficiency.[9,10,44,45] Typically for PC PeLED, the interface between MHP and the underlying layer affects the crystallization of MHP crystal.[44] Therefore, crystallization dynamics related to surface roughness, and surface energy need to be systematically studied for efficient PC PeLED fabrication.

Here, we systematically review the strategies to improve the efficiency of PeLED with device architecture engineering (**Figure 1**). Various strategies to modify HTL and ETL to overcome the issue related to charge balance, carrier injection, and interface quenching are classified and reviewed in the categories according to the Figure 1.

2. HIL and HTL Engineering

The HIL and HTL are crucial layers to promote hole injection into the light-emitting layer. The commonly used HIL is poly(3,4-ethylenedioxythiophene):polystyrene sulfonate (PEDOT:PSS), which exhibits excellent transparency and conductivity. Subsequently, other HILs such as nickel oxide (NiO$_x$)[46] and HTLs such as poly(N,N′-bis-4-butylphenyl-N,N′-bisphenyl)benzidine (poly-TPD),[47] poly(9-vinylcarbazole) (PVK)[48] with EQE over 10% have been reported for PeLEDs. Each of these materials has distinct characteristics, so their features must be clearly understood to increase the device efficiency.

For conventional LED devices, the main role of HIL/HTL can be classified to three major categories (Figure 1). The principal function of HIL/HTL is to offer energy ladder to effectively transport hole into MHP layer. However, owing to deep lying HOMO level of MHP emitting layer compared to conventional transparent electrode (e.g., indium tin oxide (ITO) and fluorine-doped tin oxide (FTO)), hole injection can be limited. Typically for blue-emitting MHP layer with deeper HOMO level, this problem became more critical. Along with proper
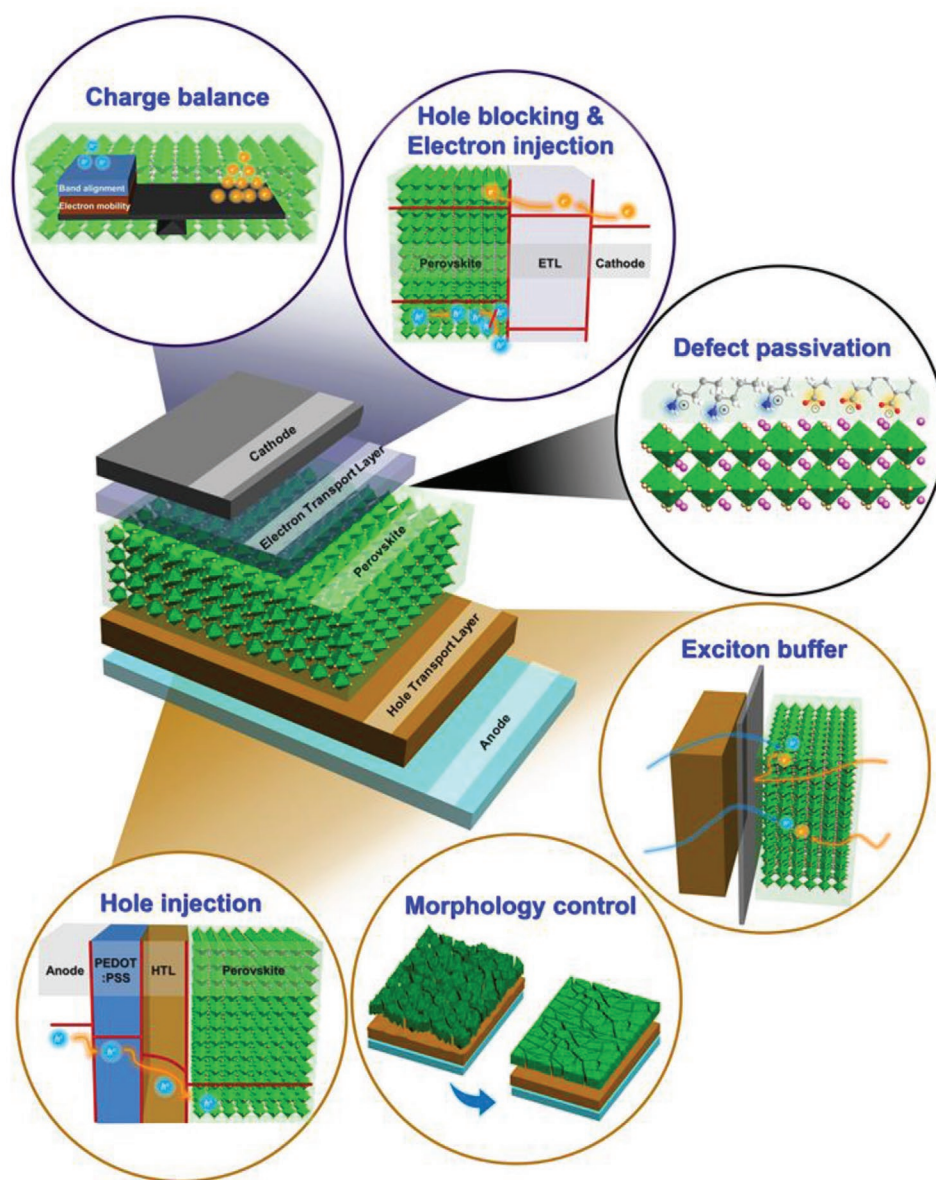
ADVANCED
SCIENCE NEWS
www.advancedsciencenews.com

ADVANCED
MATERIALS
INTERFACES
www.advmatinterfaces.de

Figure 1. Device architecture design strategies to achieve highly efficient PeLED.

energy barrier, low conductivity of HTL should be considered together because it can also result in charge imbalance. Therefore, device architecture engineering on increasing hole injection is mainly focusing on lowering hole injection barrier and attaining sufficient charge carrier mobility.

For PC PeLEDs, the wettability between HIL/HTL and MHP precursor solution is another important factor to consider for smooth MHP film. Good wettability should be satisfied for LED application. HTL with bad compatibility creates only few nucleation sites during the crystallization of MHP and thus large grain size is attained.[49] Large grain size cannot sufficiently limit the exciton diffusion and accordingly thermal ionization of electron-hole pairs can occur at room temperature.[10] Therefore, good wetting of MHP precursor solution on HIL or HTL is the prerequisite for HIL or HTL nominees.

Also, the roughness of underlying substrate impacts the creation of nucleation sites.[50] Among concave, plane, convex regions, it is thermodynamically calculated that nucleation is predominant for concave region, which shows the lowest free energy of formation.[50] As a result, pinholes can be formed inside MHP layer due to limited nucleation, which is generated preferably in the concave region.[50] Accordingly, architecture design concentrates on reducing surface energy between HTL and MHP precursor solution and gaining flat HTL to achieve efficient PeLED. Evaporation time of the polar solvent is another important factor. The swelling of the underlying polymer by a polar solvent of the precursor solution can delay the evaporation time, which provides enough processing time window to apply the NCP process at the early stage of crystallization to form smaller and granular crystals.[44]

Lastly, reducing exciton quenching is a significant task for designing device architecture. MHP have long exciton diffusion length, thus the generated exciton in MHP can be highly affected by the nonradiative recombination site at the interface. Solution processed conducting polymer HIL/MHP interface is especially important in conventional structure PeLED where ETL is mostly formed with vacuum deposition.[51–54] In case of PEDOT:PSS, acidic PEDOT etches ITO substrate and metallic indium ion can be released an consequently migrated metallic indium species in the MHP layer induce non-radiative recombination and strongly reduce the luminescence.[51] Inorganic NiO_x, another conventional HIL, is also reported to quench the PL, which is attributed to existence of non-radiative recombination in their defect sites or charge transfer process at the HIL/MHP interface.[52] Some strategies have been suggested to avoid those adverse effects from HIL.

2.1. Increase in Hole Injection

Conventional HIL, PEDOT:PSS is composed of two complementary polymers; highly conductive poly(3,4-ethylenedioxythiophene (PEDOT) and water-soluble polystyrene sulfonate (PSS). Therefore PEDOT:PSS is water-soluble, highly transparent, and conductive, which is suitable for HIL application.[55] However, PEDOT:PSS has a slightly shallow HOMO level around −5 eV, so large hole injection energy barrier to MHP layer can restrict hole injection.

Inserting additional interlayers on HIL with deeper HOMO is an effective and easily accessible approach to reduce the hole injection barrier when designing the architecture of PeLEDs. Various interlayers which will be introduced in this chapter are arranged according to their energy levels and their own function (**Figure 2**). Highly efficient green-emitting PeLEDs have been reported with additional HTL interlayers.[56–59] Fabrication of HIL with gradient WF can be alternative strategies for highly efficient PeLEDs.[9]

Mixing of deep HOMO materials with PEDOT:PSS is effective to overcome limited hole injection. Among deep HOMO materials, hydrophobic polymer perfluorinated polymeric acid, i.e., tetrafluoroethylene-perfluoro-3,6-dioxa-4-methyl-7-octene-sulfonic acid copolymer (PFI) can be chosen because the proportion of PFI gradually increases along the MHP EML direction.[9] The fluorocarbon chains in PFI make it hydrophobic, whereas the substrate is UV-O treated and hydrophilic, so during spin-coating of a solution of PEDOT:PSS and PFI, the PFI tends to segregate preferentially to the top of the HTL.[9] This surface-enrichment of PFI increases the WF of HIL from 4.9 to 5.95 eV as PFI concentration relative to the PEDOT:PSS increases (**Figure 3**a). Moreover, the PFI-enriched surface layer can also block migration of indium released from the ITO due to etching by acidic PEDOT:PSS.[9]

Doping small amount of molybdenum(VI) oxide (MoO_3) in PEDOT:PSS also have similar functional role.[60] Up to 0.7 wt% MoO_3 in the form of ammonium molybdate powder can be mixed with PEDOT:PSS and the WF is increased from 5.15 to 5.31 eV. The optimized amount of MoO_3 in PeLEDs efficiency is 0.5 wt% while excess MoO_3 increased the roughness and caused pinholes in the surface.[60] Increased roughness with excess MoO_3 possibly attributed to their low solubility into polar solvent.[60] The low solubility of MoO_3 to PEDOT:PSS can be solved by introducing ammonia solution.[61] High volume ratios up to 0.8:1 (MoO_3-ammonia: PEDOT:PSS) is achieved by mixing premixed MoO_3–ammonia solution and PEDOT:PSS. The WF is further increased to 5.6 eV at 0.8:1 volume ratio (Figure 3b).

Two-dimensional materials also can serve as a solution-processible interlayer on PEDOT:PSS. Among them, 2D black phosphorous (BP) has been widely adopted to organic and MHP solar cells, attaining enhanced power conversion efficiencies owing to its high carrier mobility and deep HOMO level of −5.32 eV.[62] Exfoliated BP flakes formed large and ultrathin film, which contributes to smooth, uniform and continuous film on PEDOT:PSS. The BP layer decreased the injection barrier and assisted uniform MHP growth, therefore BP layer had a beneficial impact on increasing EQE.[62]

Also, large hole injection barrier between HTL and MHP EML can be overcome by preferentially aligning surface dipole using amphiphilic material.[63] If an interlayer with dipole can be preferentially coated on, surface dipole can decrease the HOMO level to reduce the hole injection barrier.[63] Poly[(9,9-bis(3′-(N,N-dimethylamino)propyl)-2,7-fluorene)-alt-2,7-(9,9-dioctylfluorene)] (PFN), which has hydrophobic carbon backbones and hydrophilic protonated ammonium groups, exhibits advantageous effect on decreasing hole injection barrier.[63] When PFN is coated on a hydrophobic HTL such as PVK or poly-TPD, their backbones interact with the underlying hydrophobic substrate and hydrophilic ammonium groups became predominant on the surface.[63] This self-organization by PFN increased the hydrophilicity of the surface and simultaneously decreased the HOMO level of poly-TPD from −5.3 to −5.8 eV, which reduced energy offset and balanced bidirectional charge injection (Figure 3c).[63] Furthermore, inserting PFN interlayer on HTL achieved high crystallinity and self-organized hydrophilic ammonium group increased wettability. Because ammonium group can bind with MHP crystal, defects sites in MHP have decreased, so PFN-coated MHP films had longer PL lifetime (≈97.8 ns) than pristine films (≈46.5 ns) (Figure 3d).

Amphiphilic material is also effective to increase the WF of inorganic HIL. NiO_x is air stable inorganic HIL, which can
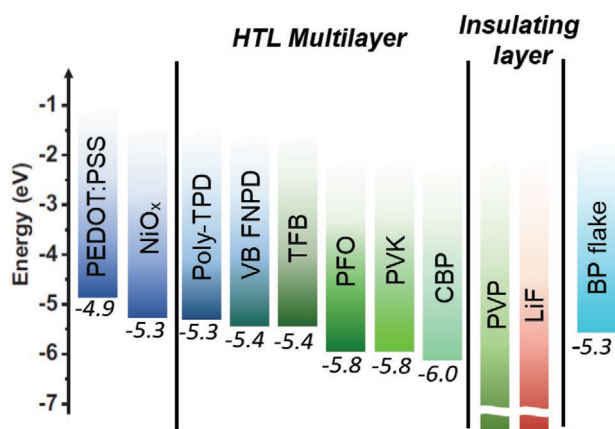

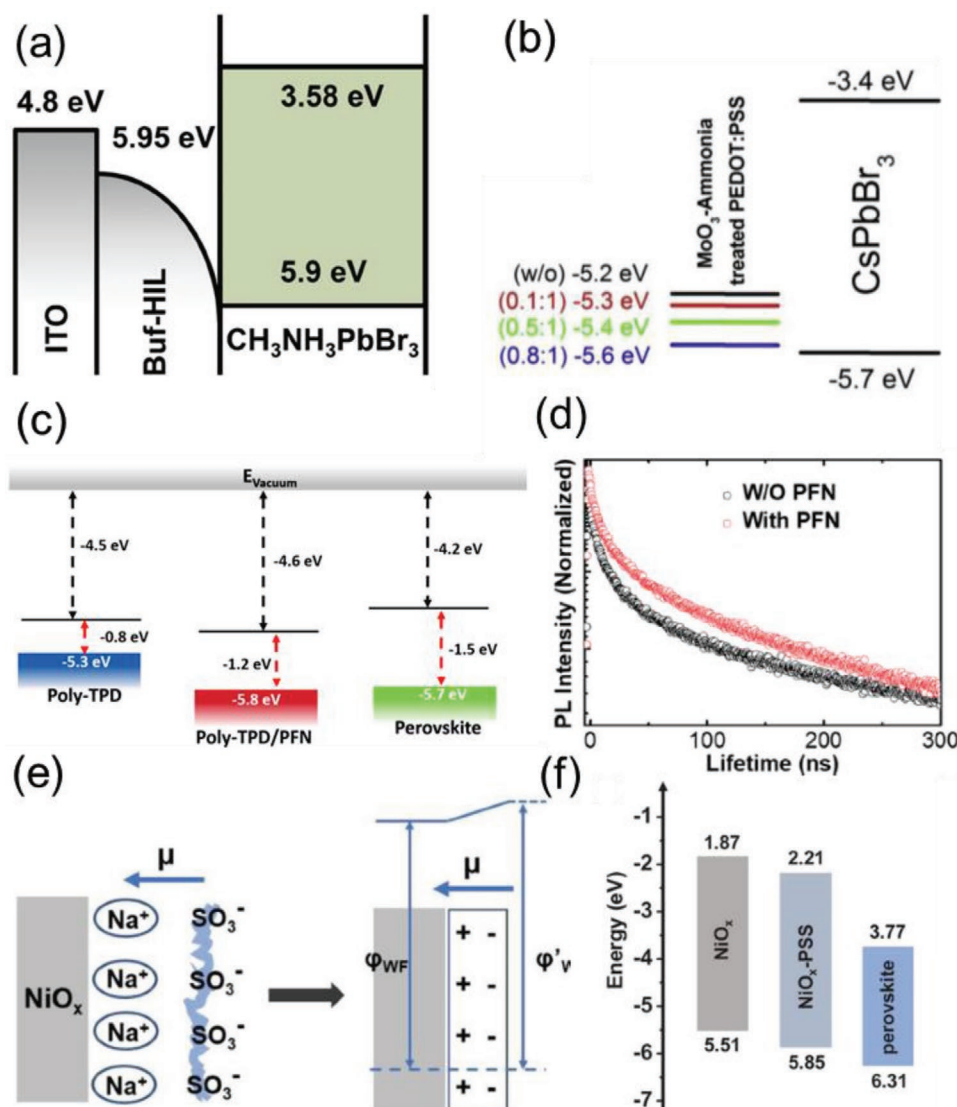**Figure 2.** Energy band diagram of the various interlayers on HTL.

ADVANCED
SCIENCE NEWS
www.advancedsciencenews.com

ADVANCED
MATERIALS
INTERFACES
www.advmatinterfaces.de

Figure 3. a) Schematic energy-level diagram of ITO/Buf-HIL/MAPbBr$_3$. Reproduced with permission.[9] Copyright 2014, Wiley-VCH. b) Energy level for MoO$_3$-ammonia treated PEDOT:PSS layers and CsPbBr$_3$ perovskites. Reproduced with permission.[61] Copyright 2018, Elsevier B.V. c) Schematic illustration of the reduced HOMO level of PFN-modified poly-TPD to lower the hole injection barrier to the perovskite layer. d) Time-resolved PL lifetime of the perovskite film deposited on a quartz substrate from the perovskite precursor solution with and without PFN additive. Reproduced with permission.[63] Copyright 2018, American Chemical Society. e) Dipole formation on NiO$_x$ by PSSNa and increased work function. f) Energy levels for NiO$_x$, NiO$_x$-PSSNa, quasi-2D perovskite of CsPbBr$_3$ with propylamine hydrobromide. Reproduced with permission.[53] Copyright 2019, Wiley-VCH.

enhance the device stability. However, their low WF (4.86 eV) and shallow HOMO level (−5.31 eV) restrict their use for PeLED. Energy level could be controlled by treating amphiphilic PSS-Na on NiO$_x$.[53] The Na$^+$ in PSS-Na preferentially toward NiO$_x$, and the SO$_3^-$ of PSS-Na orients toward the MHP layer, and preferential orientation of PSS-Na creates a dipole moment toward NiO$_x$ (Figure 3e). As a result, the dipole moment of PSS-Na deepens the HOMO level to −5.85 eV (Figure 3f). This change is compatible with the deep-lying HOMO of the blue-emitting MHP. Additionally, this surface treatment with PSS-Na additionally reduced the r_{RMS} and increased the average PL lifetime.[53]

For inorganic metal oxide NPs, it is also possible to adjust their WF with ligand engineering without adop-tion of additional amphiphilic interlayer. Cuprous oxide (Cu$_2$O) is a p-type metal oxide that has high hole mobility (μ_h) and long carrier-diffusion length. To engineer the band edges of Cu$_2$O NPs, ligand passivation with various functional groups has been presented.[64] The ligands did not penetrate or change the crystallinity of the upper CsPbBr$_3$ nanocrystals, but the surface is modified after ligand treatment on Cu$_2$O NPs. The optical bandgap remained near 2.1–2.2 eV, but each ligand up-shift the band energy of Cu$_2$O.[64] For instance, Cu$_2$O NPs capped with 1,2-ethanedithiol showed slightly upshifted band energy because the interfacial dipole moment offset the intrinsic dipole that occurs due to the presence of thiol ligands. Cu$_2$O NPs capped with tetrabutylammonium chloride showed a

large interfacial dipole between the surface and ligand rather caused deeper band-edge energies.[64] Those trends imply that band energy can be controlled by appropriate ligand selection while keeping bandgap unchanged. Under the trade-off between the insulating nature of ligand and bandgap adjustment to reduce the hole-injection barrier, ligands in Cu_2O affect the current–voltage characteristics.[64] Metal oxide NPs have shown high potential for use as an HIL or HTL for efficient and stable PeLEDs, and increased understanding of the surface dipole between ligand and NPs might guide engineering of its band energy and hole injection.

2.2. Morphological Engineering by an Interlayer to Increase Surface Wettability

For PC PeLEDs, the MHP layer is generally crystalized from the precursor dissolved in a polar solvent such as N,N-dimethylformamide (DMF) and dimethylsulfoxide (DMSO). Therefore, on the hydrophobic substrate, many pinholes or defects can be generated in MHP during the crystallization due to poor surface wettability. To employ the MHP film as an EML for PeLEDs, the film is required to achieve relatively thinner thickness compared with that of the active layer for MHP solar cells to maximize light outcoupling and reduce self-absorption. Therefore, the control of surface wettability of MHP precursor solution on HIL/HTL is of importance to attain thin and smooth MHP films.

The morphological issue caused by bad surface wettability can be resolved by introducing a ultra-thin (<5 nm) hydrophilic interlayer on hydrophobic surface that makes the surface hydrophilic. Insertion of a thin polyvinylpyrrolidone (PVP) layer on ZnO exhibited superior surface morphology with less pinholes for inverted structure PeLEDs.[65] The increased hydrophilicity with the PVP interlayer is confirmed by the fast spreading of MHP precursor solution with real-time contact angle analysis. Without the PVP interlayer, the droplet of MHP precursor solution kept its original circular shape until 0.4 s, however the droplet gradually spread radially on the surface with the PVP modification (**Figure 4**a,b).[65] Planar SEM images of the MHP film with the PVP layer illustrated much smoother and denser film morphology with fewer pinholes than those of the control film. The reduced density of defects contributed to increasing PL intensity and PL lifetime owing to suppressed nonradiative recombination.[65] This ultrathin coating of the PVP interlayer is so versatile that it also can be adopted as an interlayer on a conventional PEDOT:PSS layer to smoothen the PEDOT:PSS/MHP interface.[66]

Even though a hydrophilic polymer interlayer increase surface wettability, some portion of the PVP interlayer can be washed away while depositing an overlying MHP layer because both PVP and the MHP precursor are dissolved in DMSO. In this case, atomic layer deposition (ALD)-processed metal oxide can be another option to solve the morphological problem. Uneven surface that originated from multiple solution-processing of HTLs is smoothened with low-temperature deposition of a thin Al_2O_3 interlayer on poly[(9,9-dioctylfluorenyl-2,7-diyl)-co-(4,′-(N-(4-sec-butylphenyl)

diphenylamine)] (TFB)/PVK.[67] For ITO/TFB/PVK films in Figure 4c, the patchy circular pattern corresponds to thinner HTL (TFB) with higher mobility (Figure 4c). However, the circular pattern disappeared after depositing Al_2O_3 on TFB/PVK because Al_2O_3 entirely covered the film (Figure 4d). Furthermore, as ALD cycle numbers increase, water contact angles gradually decrease from 90.2° (TFB/PVK) to 72.1° (TFB/PVK/Al_2O_3, cycle number = 70) which induces better wettability of the MHP precursor on the surface of the HTLs. Enhanced wettability is also proven by increased surface tension of substrate from 19.83 mJ m^{-2} (ITO/TFB/PVK) to 34.13 mJ m^{-2} (ITO/TFB/PVK/Al_2O_3, cycle number = 70), which resulted in high-quality MHP films.

Similarly, uneven surface of PEDOT:PSS, which resulted from a segregation of PSS chains, can be covered by ultrathin LiF interlayer of 1–4 nm.[68] The LiF is generally deposited between ETL and electrode to increase electron injection.[69] However, the LiF interlayer is beneficial even on a PEDOT:PSS layer. When 1 nm thick LiF is deposited on PEDOT:PSS, high RMS roughness of pristine PEDOT:PSS (2.48 nm) largely decreased to 1.29 nm.[68] Also, the voids and pinholes on ITO/PEDOT:PSS disappeared on ITO/PEDOT:PSS/LiF for all of LiF deposited films, which is attributed to enhanced wettability confirmed by lower contact angles of mixed DMF/DMSO on LiF interlayer compared to pristine PEDOT:PSS (Figure 4e).[68] However, as LiF layer became thicker from 1 to 4 nm, the grains became aggregated and crystallinity was reduced, thereby increasing RMS roughness, and the insulating property of LiF significantly hindered hole injection (Figure 4e).[68] The LiF interlayer approach is quite versatile that the surface of NiO_x can also become hydrophilic with modification of LiF.[70] The thin LiF layer has the merit of better surface wettability with the MHP precursor solution than other materials such as PVK, TFB, and poly-TPD. The contact angles of MHP precursor solution on PVK, NiO_x, NiO_x/LiF were 52.9°, 17.2°, 22.9°, respectively.[70] In case of PVK, bad wettability caused uneven surface morphology, and, NiO_x, NiO_x/LiF revealed similar contact angle with well coated MHP films. Use of a LiF interlayer can reduce exciton dissociation and keep surface wettability.

2.3. Preventing Exciton Quenching at HIL/MHP Interface

2.3.1. Exciton Buffer Layer

Conventional HIL such as PEDOT:PSS and NiO_x can quench the exciton at the interface between HIL and EML. Especially in PeLED, PEDOT:PSS and NiO_x induce significant exciton quenching and thereby reduce the device efficiency due to a long exciton diffusion length of MHP. Also, acidic PEDOT:PSS can etch the metal oxide electrode (e.g., ITO, FTO) and diffused metallic species can be exciton quencher at the interface. Therefore, strategies to overcome the intrinsic exciton quenching at the PEDOT:PSS need to be provided.

The key point of buffering exciton is to block direct contact between MHP EML and conductive PEDOT polymer. Therefore a self-organized PEDOT:PSS helps to reduce exciton quenching at the interface and facilitates hole injection with excess PSS
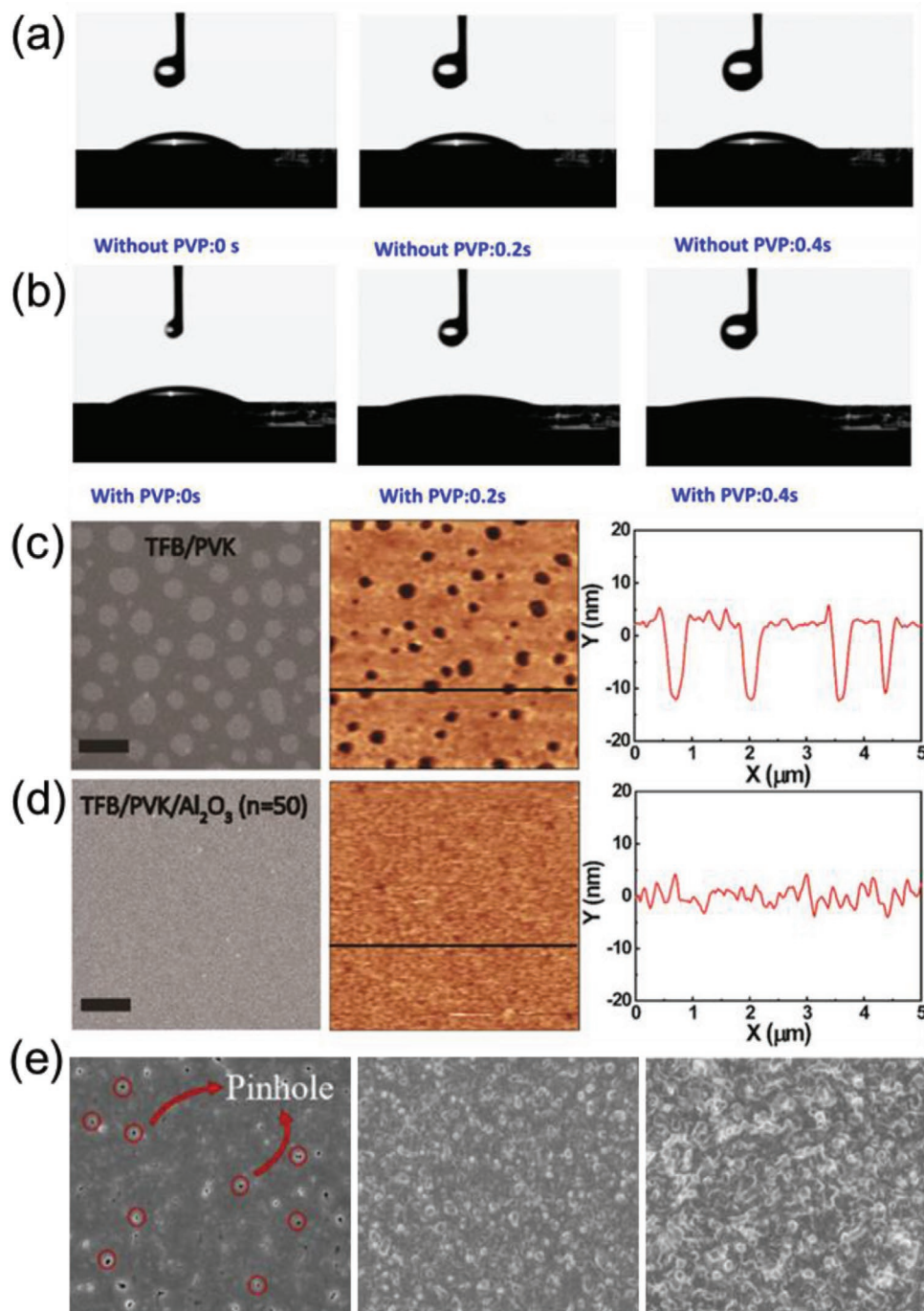
ADVANCED
SCIENCE NEWS
www.advancedsciencenews.com

ADVANCED
MATERIALS
INTERFACES
www.advmatinterfaces.de

Figure 4. Real-time contact angle measurements for H$_2$O deposited onto a) ZnO and b) ZnO/PVP surfaces. Reproduced with permission.[65] Copyright 2017, Nature Publishing Group. c) AFM height and line scans of ITO/TFB/PVK. The scan area of the AFM image is 5 μm × 5 μm. d) AFM height and line scans of ITO/TFB/PVK/Al$_2$O$_3$ (cycle number = 50). The scan area of the AFM image is 5 μm × 5 μm. Reproduced with permission.[67] Copyright 2020, American Chemical Society. e) Top view scanning electron microscope (SEM) images of perovskite films on ITO/PEDOT:PSS/LiF of 0, 1, 4 nm, respectively. Reproduced with permission.[68] Copyright 2020, Elsevier B. V.

ratio in PEDOT:PSS. A PSS-enriched surface can be achieved by additional of sodium-poly(styrenesulfonate) (Na-PSS) onto the PEDOT:PSS layer.[71] Due to the vertical segregation of PEDOT and PSS, a highly PSS-enriched overlayer is formed at the surface of PEDOT:PSS; consequently the HOMO level is decreased from −4.9 to −5.2 eV, so hole injection is improved.[71,72] Moreover, decreased direct contact between PEDOT and MHP EML

significantly increased steady-state PL of MAPbBr$_3$ on Na-PSS by 10 times compared to PEDOT:PSS. However, PSS is a less conductive polymer compared to PEDOT, this PSS-rich surface can result in inferior hole injection. In some cases, use of additional interlayer on PEDOT:PSS enhanced EQE by blocking exciton dissociation in spite of increased charge imbalance.[54] Two poly(triarylamine) interlayers, i.e., TFB and poly-TPD, are

**ADVANCED
SCIENCE NEWS**

www.advancedsciencenews.com

**ADVANCED
MATERIALS
INTERFACES**

www.advmatinterfaces.de

separately coated on PEDOT:PSS to reduce nonradiative recombination at the PEDOT:PSS/MHP nanoplatelets interface.[54] Comparison of electron injection in electron-only device to that of hole injection in hole-only device illustrates electron injection dominates over hole injection. This electron dominant tendency even became larger with addition of TFB and poly-TPD interlayer.[54] However, blue-emitting PeLEDs exhibited EQE$_{max}$ of 0.3% and 0.55%, which are almost twice as high as those of control devices, which implies that both(triarylamine) polymers significantly decreased non-radiative channels and thereby reduced exciton quenching.[54]

The interface between NiO$_x$ and MHP EML also should be handled to block nonradiative decay channels, which hamper radiative recombination.[52] This could be handled with insertion of PVK interlayer.[73] NiO$_x$/PVK films yield a smooth surface with small RMS roughness r_{RMS} = 0.9 nm than pristine NiO$_x$ (r_{RMS} = 2.2 nm), so consequently the PVK interlayer increased the smoothness of the crystallized MHP layer. Furthermore, MHP films on NiO$_x$/PVK had longer average PL lifetime (95.4 ns) than films on NiO$_x$ (47.9 ns). Green light emission on NiO$_x$/PVK is uniform and bright, while NiO$_x$ substrates showed numerous dark spots. Insertion of PVK interlayer between EML and NiO$_x$, which offers exciton decay paths, decreased nonradiative exciton recombination by blocking direct contact.[73] PVK without a NiO$_x$ layer has poor hole injection from the ITO due to the large energy barrier between ITO and PVK, so NiO$_x$/PVK as a multilayer HTL is necessary.[73] The laddered structure of NiO$_x$/PVK provided green-emitting quasi-2D PeLEDs that had an EQE$_{max}$ = 11.2%, which is greater than those of PeLEDs that used a single layer of neat PVK (7.05%) or NiO$_x$ (3.07%).[73]

2.3.2. Alleviating the Acidic Nature of PEDOT Polymer

MoO$_3$-ammonia mixing treatment prevents exciton quenching by metallic species that migrate into MHP EML.[61] The pH of MoO$_3$-ammonia treated PEDOT:PSS increased from ≈2.08 to ≈11.73; this increased basicity prevents the electrode etching from acidic of PEDOT:PSS. The concentration of indium in ITO surface decreased from 16.38% to 7.81% when an ITO surface is washed using acidic PEDOT:PSS, but remained at 16.54% when washed with mildly-basic PEDOT:PSS that had been treated using MoO$_3$-ammonia.[61] In short, ammonia solution not only increased solubility of MoO$_3$ but also reduced indium migration from ITO by neutralizing PEDOT:PSS. Meanwhile, acidic nature of PEDOT can be effectively eliminated by replacing PEDOT with similar functional polymer. Substitution of PEDOT with less acidic polyaniline reduced ITO etching, thus reduced the luminescence quenching of PeLEDs.[44] In poly(styrenesulfonate)-g-polyaniline (PSS-g-PANI), two polymers, PSS and PANI, are covalently bonded to each other (**Figure 5**a), whereas PEDOT forms ionic bonds with PSS in PEDOT:PSS (Figure 5b). Therefore, PSS-g-PANI is soluble in polar solvent. PSS-g-PANI can be slightly swollen with DMSO during spin-coating of MHP precursor solution, so evaporation of DMSO is delayed during spin-coating process and the crystallization time is longer for PSS-g-PANI/MAPbBr$_3$ (≈170 s) than for PEDOT:PSS/MAPbBr$_3$ (≈120 s).

Slow crystallization contributes to formation of smooth and highly oriented MAPbBr$_3$ film, which provide wider processing window of the films when NCP process is applied on the quasi-film (Figure 5c). The relationship between solvent evaporation rate and morphology is well explained by LaMer's nucleation theory (Figure 5d): when a solvent evaporates continuously, the concentration of the solution increases and finally reaches supersaturation concentration C_s; however, a higher minimum nucleation concentration $C_{nu,min}$ than C_s must be attained to get enough energy to overcome the nucleation barrier and subsequently enable growth of nuclei. The slowing of DMSO evaporation by PSS-g-PANI increases the time taken to attain C_s and increases the nucleation period, so grain size is larger than in PEDOT:PSS (Figure 5e).[44] The large and flat MHP layer obtained using PSS-g-PANI without NCP process can be beneficial for separation of electron–hole pairs in MHP solar cells but not for efficient emission in PeLEDs. Therefore, additive-based NCP process using a chloroform solution containing a very small amount of 2,2′,2″-(1,3,5-Benzinetriyl)-tris(1-phenyl-1-H-benzimidazole) (TPBi) is applied on the quasi-film to make uniform small nanograin MHP films. Unlike the solvent dripping process in MHP solar cells, nonvolatile solvent is essential to induce fast crystallization to finish the grain growth. Finally, small nanograins in the films are achieved to confine the excitons spatially. The PL intensity of MHP films on ITO/PSS-g-PANI is similar with that on bare ITO and much stronger than that on PEDOT:PSS.[44] The difference between the PL intensity of PSS-g-PANI and PEDOT:PSS is a result of reduced migration of indium species in PSS-g-PANI, because it is not as acidic as PEDOT:PSS and does not etch the ITO electrode much. The PeLEDs with polycrystalline MAPbBr$_3$ showed much increased EQE$_{max}$ of 2.96% on PSS-g-PANI, and EQE$_{max}$ of 1.47% on PEDOT:PSS. Furthermore, PeLEDs with FAPbBr$_3$ NPs also had increased EQE$_{max}$ of 7.73% from EQE$_{max}$ of 5.58%.

2.3.3. Substituting ITO Substrate to Conductive Polymer Anode (CPA)

Metallic species can be much stronger luminescence quenching centers in PeLEDs than in OLEDs, which can be ascribed to much larger exciton diffusion length of MHPs than of organic semiconductors.[10] Migration of indium from ITO upon exposure to acids or during device operation is inevitable, but can be avoided by replacing ITO with a CPA on top of glass.[74] An ideal CPA as an anode should have high WF and high conductivity (κ) at the same time. However, most of additives to increase the κ in CPA reduces the WF and most of additives to increase the WF in CPA decrease the κ. Therefore, there has been a trade-off between WF and κ upon adding additives into the CPAs. An anode composed of a self-organized conducting polymer, mixture of PEDOT:PSS and PFI, has an WF that increases gradually from 4.73 to 5.8 eV.[9] This continuous and gradually formed band energy helped to inject holes into MAPbBr$_3$ PC films. The CPA is further improved by mixing DMSO and MAX (X = I, Br) into mixture of PEDOT:PSS ad PFI (**Figure 6**a).[74] A CPA with high conductivity κ > 1400 S cm^{-1} and high WF ≈ 5.85 eV is achieved by
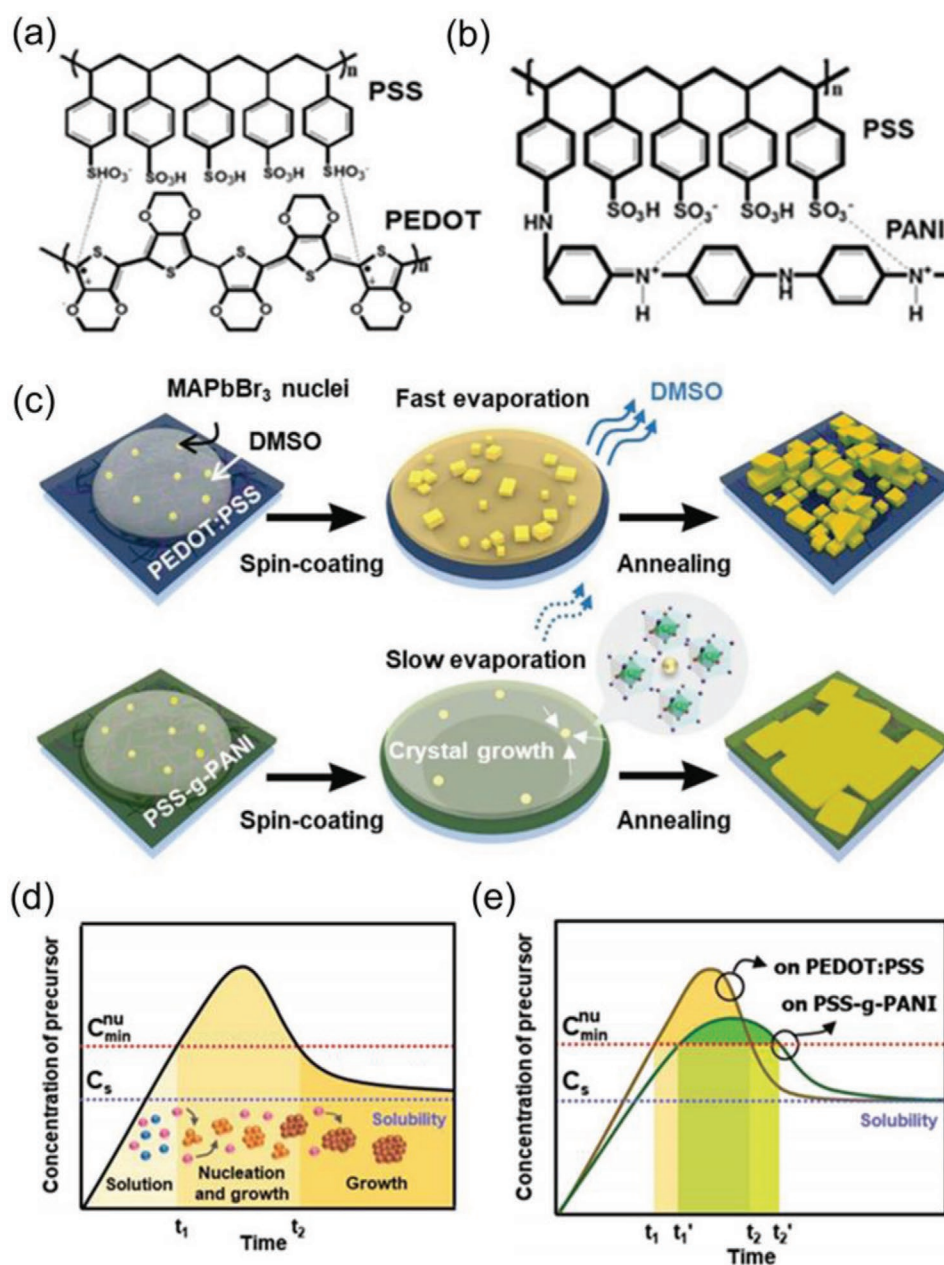
Figure 5. Chemical structure of a) PEDOT:PSS and b) PSS-g-PANI. c) Schematic diagram of spin-coating process for MAPbBr$_3$ films on PEDOT:PSS and PSS-g-PANI. d) LaMer diagram. e) MAPbBr$_3$ crystallization on PEDOT:PSS and PSS-g-PANI based on modified LaMer diagram. Reproduced with permission.[44] Copyright 2018, Wiley-VCH.

overcoming the trade-off between WF and κ by applying a thorough understanding of the polymeric structure of PEDOT:PSS (Figure 6b). Doping of PEDOT:PSS with only DMSO yielded low conductivity ≈868.31 S cm^{-1}, whereas codoping with MAI/DMSO or MABr/DMSO yielded superior conductivity of 1270 and 1408 S cm^{-1}, respectively (Figure 6c); the increase is attributed to enhanced π–π stacking of PEDOT chains,[74–76] which yields transformation of the resonant structure of the thiophene ring in the PEDOT chains from benzoid to quinoid structure; this change increases the linearity of conjugated chains, and increases the number of delocalized electrons and thereby contributes to increased conductivity (Figure 6d,e). To

summarize, MABr/DMSO and MAI/DMSO additives diminished electrostatic interaction between PEDOT and PSS by separately combining with charged PEDOT$^+$ and PSS$^-$.[74] Therefore, π–π stacking of PEDOT became prominent, and the PEDOT conformation became increasingly linear, so its κ increased.[74] κ can be decoupled from WF by adding MAX into the PEDOT:PSS:PFI CPA. With a well-modified CPA layer, PeLEDs with PC MAPbBr$_3$ had high EQE$_{max}$ = 10.93% with low V_{on} and narrow FWHM ≈ 20 nm, device half-lifetime at initial luminance at 100 cd m^{-2} is increased from 1.6 h (only-DMSO) to 5.0 h (MAI/DMSO), and overshoot tendency during device operation is decreased.

**ADVANCED
SCIENCE NEWS**

www.advancedsciencenews.com

**ADVANCED
MATERIALS
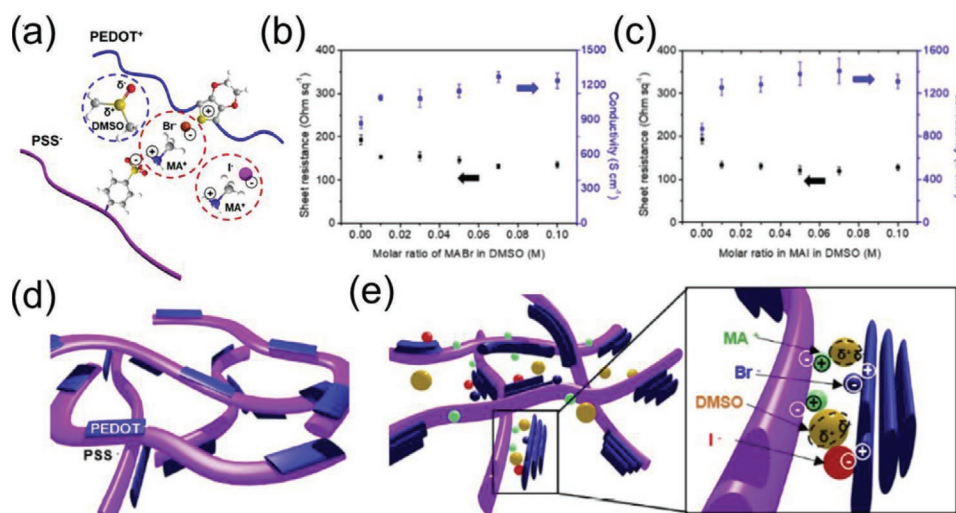INTERFACES**

www.advmatinterfaces.de

Figure 6. a) Schematic illustration of reduced Coulombic interaction between PEDOT and PSS by DMSO, MABr, and MAI additives. b) Sheet resistance and c) conductivity of PEDOT:PSS films with varying ratios of MABr and MAI. Schematic illustrations of PEDOT$^+$ and PSS$^-$ chains d) before and e) after addition of ammonium halide/DMSO additives. Reproduced with permission.[74] Copyright 2019, Elsevier Ltd.

2.4. HIL/HTL Interfacial Engineering to Enhance Light Outcoupling

Even though the PLQY of MHP have achieved near unity,[29] low η_{out} for PeLEDs is a significant hurdle to achieve highly efficient PeLEDs. Because MHP possesses higher refractive index than organic light-emitting materials, the optimized device structures of PeLEDs for better outcoupling can also be different from those in OLEDs.[77] Among the layers which comprises normal structured PeLEDs, HIL/HTL possesses large portion for better light outcoupling because those are relatively thicker than the emitting layer and light escapes sequentially through the HTL, HIL and transparent electrode. It is theoretically calculated that the refractive index, thickness and surface pattern of HTL are crucial factors to maximize light outcoupling.[77]

In terms of refractive index, the large difference of the MHP EML and substrate causes the loss of generated photons in waveguide and substrate mode, therefore matching the refractive index at the interfaces of PeLEDs should be considered. For instance, the Al_2O_3 interlayer on TFB/PVK have increased η_{out} at wavelength of 514 nm by reducing refractive index gap.[67] The refractive index of Al_2O_3 is located between PVK and $CsPbBr_3$, so decreased refractive index difference alleviates reflection at the interface. The η_{out} at 514nm with pristine TFB/PVK layer was 24.8%, and η_{out} of a maximum value of 26.9% was achieved with insertion of a Al_2O_3 layer (cycle number = 10). After the maximum point of η_{out}, it gradually declined when Al_2O_3 became thicker with large cycle number (30, 50, 70).[67] This implies that HTL thickness also significantly impact on η_{out} along with refractive index. The impact of thickness of PEDOT:PSS on light outcoupling was also demonstrated by delicate thickness control.[78] Optical simulation suggested that a thin PEDOT:PSS layer (≈6.9 nm) is appropriate in the range of green emission region to boost the EL intensity because there is nontrivial extinction coefficient at 520 nm in PEDOT:PSS layer (**Figure 7**a).[78] The ultrathin PEDOT:PSS can be applied

to various MHP EMLs such as 3D, quasi-3D (or 2D/3D hybrid) and quasi-2D with different ratio of large ammonium cation. The 3D, quasi-3D, quasi-2D PeLEDs based on UT-PEDOT:PSS achieved EQE_{max} = 17.6%, 15.0%, and 6.8%, which are 1.42, 1.87, and 2.11 times higher than in counterpart devices that used conventional PEDOT:PSS.[78]

The η_{out} can be also improved by incorporating nano-patterns on an HIL or an HTL. For example, the use of bioinspired moth-eye nanostructures (MEN) enhances η_{out} with suppression of the Fresnel reflection at the interface, attaining high optical transmittance at broad wavelength.[79] The MEN-imprinted PeLEDs are fabricated by applying compressive stress on sol-gel-derived zinc oxide (ZnO) layer with MEN patterned poly(dimethylsiloxane) mold. With a patterned ZnO/PEDOT:PSS hole injection layer, the optical transmission increased to achieve nearly 90% over a wide spectral range owing to gradiently formed refractive index of the subwavelength nanostructures (Figure 7b).[79] Also, haze values, which represents the percentage of scattered light compared to transmitted light, largely decreased for patterned ZnO/PEDOT:PSS bilayer (5.2%) compared to the patterned ZnO without PEDOT:PSS (9.0%) (Figure 7b). The optical simulation of near-field light intensity at 514 nm for flat and patterned devices illustrates that outcoupling loss is dominant in case of the flat devices owing to large refractive index difference between ZnO and PEDOT:PSS (Figure 7c).[79] However, MEN-patterned devices let trapped light to scattered out and reached 1.93 times increased calculated outcoupling efficiency, leading to 1.51 times EQE_{max} increment to 20.3% (Figure 7d).

3. Defect Passivation Layer

Theoretical calculations suggest that most of the defects generated in MHP crystals are shallow, and cannot induce nonradiative recombination.[80,81] However, many experimental results suggest that passivation of defects in MHP can
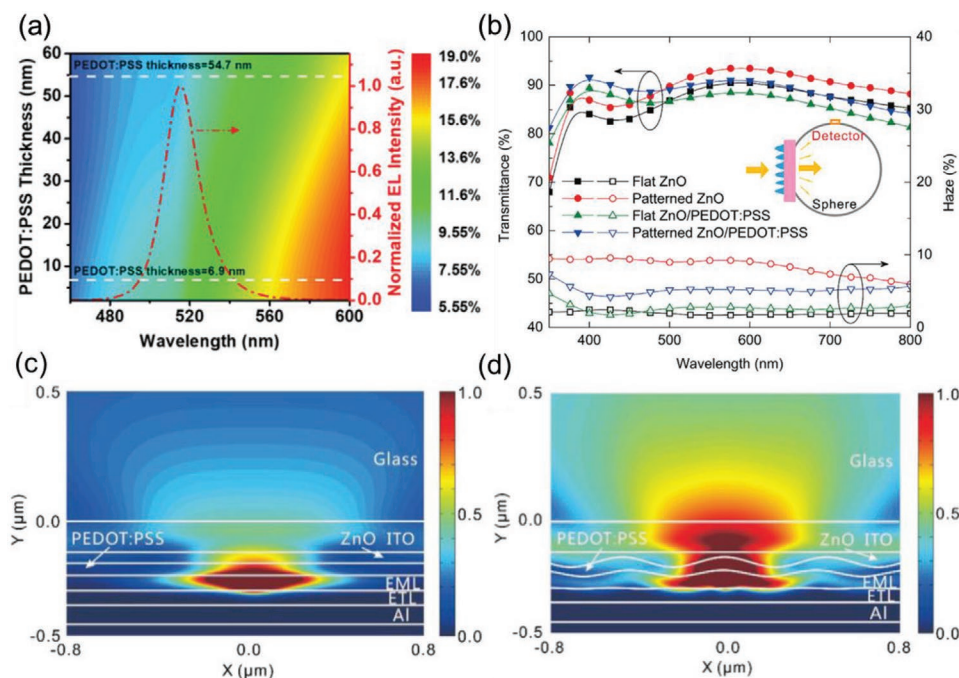
ADVANCED
SCIENCE NEWS
www.advancedsciencenews.com

ADVANCED
MATERIALS
INTERFACES
www.advmatinterfaces.de

Figure 7. a) The light extraction efficiency of PeLEDs as a function of PEDOT:PSS thickness and emission wavelength. Reproduced under the terms of the Creative Commons CC-BY license.[78] Copyright 2020, The Authors, published by Wiley-VCH. b) Total transmittance and haze of flat and MEN-patterned substrates. The inset represents the optical measurement at the ITO side. c,d) Normalized near-field intensity distributions of the transverse electric polarized light at 514 nm c) of the flat devices, and d) of the MEN-patterned devices. Reproduced with permission.[79] Copyright 2019, Wiley-VCH.

increase the PLQY.[82–85] Furthermore, defects can allow penetration of moisture or oxygen, which initialize various mechanisms of degradation in MHP crystals.[86,87] Especially, ionic defects such as halide vacancies can significantly reduce the activation energy for ion migration,[88] and cause degradation of PeLEDs under applied bias. Therefore, to achieve highly efficient and stable PeLEDs, defects in the MHP layer must be passivated.

Defects can be most easily generated on the surface of as-deposited MHP crystal, so defect passivation at the interface between MHP crystal and above layer can be an effective method to reduce the number of dangling bonds in the MHP. Interface passivation can be achieved by overcoating with a passivation material; this method has been widely studied to increase the efficiency of optoelectronic devices. For example, in MHP solar cells, surface-passivation strategies that use various halide compounds have reduced the number of defects, and to enable fabrication of efficient photovoltaic devices. Examples include phenylethylammonium iodide,[89] quaternaryammonium iodide,[90] and phenylalkylammonium iodide.[91]

Perovskite nanoparticles (PeNPs) synthesized without any capping agent showed severe PL quenching behavior and each NP showed the blinking phenomenon.[92] However, passivation using a Lewis base such as pyridine reduced the frequency of blinking, and significantly increased the PL intensity.[92–94] This result suggest that the Lewis base ligand can effectively bind with MHP crystal by donating an electron to the MHP core, most probably to Pb sites, and thereby reduce the number of dangling bonds in the MHP crystal.[94] Similarly, a Lewis acid such as phenyl-C61-butyric acid methyl ester (PCBM)

or iodopentafluorobenzene, can show passivation effect by accepting an electron from PbX_3^- or from an undercoordinated halide ion (**Figure 8**a).[95,96] Therefore, general electron accepting/donating ligand compounds can be applied as a passivation layer to increase electroluminescence efficiency.

Octylamine, one of the passivating agent, eliminated metallic Pb after being spin coated onto MHP that had been crystallized from a precursor solution of CsBr, $PbBr_2$, and PEABr.[95] This result indicates that the MHP is effectively passivated.[10,97] Consequently, PLQY is increased from 28.6% to 59.6%, and FWHM is decreased from 27 to 24 nm, possibly due to elimination of shallow traps. An octylamine concentration of 0.5 µL mL^{-1} optimized the trade-off between passivation effect and inhibition of charge transport from the insulating carbon chain of octylamine, and increased the EQE_{max} of the PeLED from 7.0% to 11.1%.[95]

Compounds that have multiple amine functional groups can be effective passivators due to the relatively small number of insulating components. Small molecules have a greater effect than polymers that have similar chemical structure. For example, ethylenediamine can deeply penetrate into the MHP crystal, and therefore, compared to polyethyleneimine, which has a similar structure, showed more efficient passivation effect, higher PL, lower amplified spontaneous emission threshold, longer PL lifetime, increased efficiency and stability of PeLEDs.[98] Passivation by ethylenediamine also reduced blinking; this result indicates that the PL blinking phenomenon in MHP is related to electronic traps on the MHP crystal surface and can be effectively suppressed by passivation.[93,99,100] This result is consistent with the ligand effect in colloidally synthesized PeNPs (Figure 8b,c).[98]
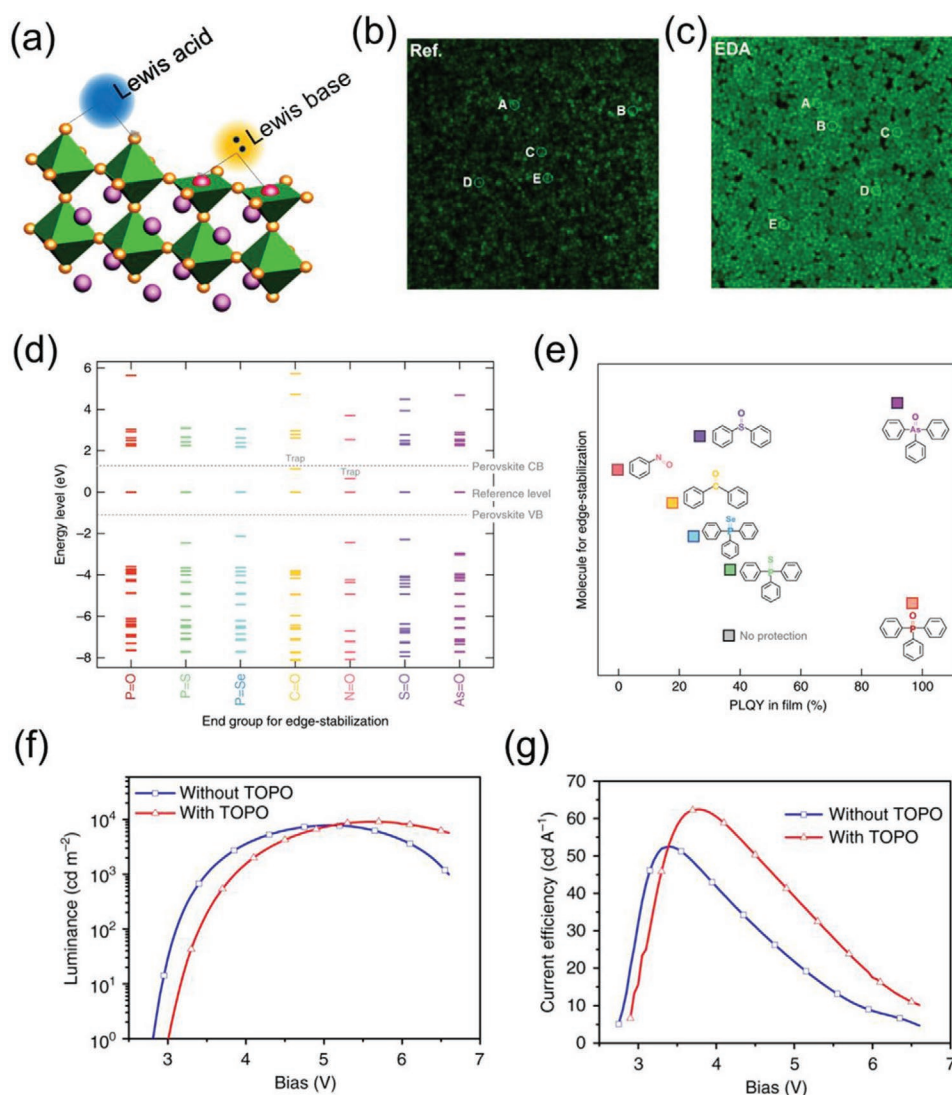
Figure 8. Defect passivation layer on perovskite layer. a) Mechanism of passivation with Lewis acid or Lewis base on perovskite layer. Confocal PL images of MAPbBr$_3$ b) without and c) with EDA passivation layer. Reproduced with permission.[98] Copyright 2017, American Chemical Society. d) Theoretical calculation of energy level and e) experimental PLQY result with oxygen sources with various termination. Reproduced with permission.[29] Copyright 2020, Nature Publishing Group. f) Luminance and g) current efficiency of PeLED with and without TOPO passivation layer. Reproduced with permission.[83] Copyright 2018, Nature Publishing Group.

Oxygen is another electron-donating passivation element that can bind with undercoordinated Pb. The passivation effect of various oxygen sources with M=O termination (M = C, N, S, P, Se) have been compared in reduced-dimensional MHP.[29] Triphenylphosphine oxide (TPPO, P = O termination) showed outstanding passivation effect, both theoretically (Figure 8d) and experimentally (Figure 8e) with high PLQY of 97%.[29] This effective passivation arises from strong binding energy of P=O:Pb (1.1 eV).[29]

Trioctylphosphine oxide (TOPO) has been used as a passivation layer to increase PLQY and extend carrier lifetime in polycrystalline MHP.[101] TOPO is an insulator, so when used as a passivation layer it decreased the injected current density to a green-emitting MHP, but increased the efficiency of PeLEDs from 52.5 to 62.4 cd A^{-1} without sacrificing maximum brightness (Figure 8f,g).[83]

4. Electron Transport Layer

The ETL is deposited on an MHP EML to facilitate electron injection and to confine holes and excitons in the MHP EML. An ETL usually has high electron mobility (μ_e) and an adequate LUMO level to decrease the electron injection barrier between EML and cathode. The low-lying HOMO level and large bandgap are important for ETL because it must also block holes and excitons. A deep HOMO level of ETL provides the energy barrier between EML and ETL, so holes accumulate at the EML/ETL surface, and exciton recombination probability can be increased.[102] Also, the large bandgap of an ETL confines excitons in the EML, and prevents emission from ETL.

The conduction band minimum (CBM) level of MHP is mostly deeper than the LUMO of the conventional organic ETL,

**ADVANCED
SCIENCE NEWS**

www.advancedsciencenews.com

**ADVANCED
MATERIALS
INTERFACES**

www.advmatinterfaces.de

so the electron injection barrier into MHP EML is negligible. On the other hand, the energy barrier from cathode to ETL, and μ_e of the ETL influences on electron injection in PeLEDs. Also, to choose the electron transport materials, the electronic properties of the HTL and EML must be considered simultaneously to make good electron–hole balance in PeLEDs.

4.1. ETL Engineering for Charge Balance

4.1.1. Electron Transport Materials and Structural Modifications

Although most of the highly efficient PeLEDs use the conventional ETL material TPBi,[20,56,103] other ETL materials such as 3,3′,3″-[Borylidynetris(2,4,6-trimethyl-3,1-phenylene)] tris[pyridine] (3TPYMB),[104] 1,3,5-Tris(3-pyridyl-3-phenyl) benzene (TmPyPB),[105] 4,6-Bis(3,5-di(pyridin-2-yl)phenyl)-2-methylpyrimidine (B2PYMPM),[43] 4,6-Bis(3,5-di(pyridin-3-yl) phenyl)-2-methylpyrimidine (B3PYMPM),[22,43,106] 2,4,6-tris[3-(diphenylphosphinyl)phenyl]-1,3,5-triazine (PO-T2T)[107] have been widely studied for further improvement of device efficiency. For example, replacement of TPBi with 3TPYMB doubled the CE compared to PeLEDs that used TPBi (6.16 to 13.02 cd A^{-1}).[104] The improvement is attributed to deep LUMO level of 3TPYMB (−3.3 eV) that facilitates electron injection and deep HOMO level (−6.8 eV) that effectively confines charge carriers in the MHP EML. Also comparable μ of HTL (poly-TPD) and ETL (3TPYMB) induces balanced charge injection to increase the efficiency.[104] Besides, CsPbBr₃/MABr PeLED have been reached EQE$_{max}$ = 20.3% using B3PYMPM.[22] There are no general superior ETL materials for all PeLEDs.

Therefore, selection of ETL must consider other layers such as EML and HTL.

Mixing ETL materials or using a multilayer ETL may be a good method to precisely control the electron injection. B3PYMPM/TPBi mixed ETL is an example. When the TPBi as an ETL was replaced with B3PYMPM, V$_{on}$ is reduced to 2.6 V and maximum luminance L$_{max}$ increased to 24 410 cd m^{-2}, which indicates the increased electron injection through B3PTMPM ETL, because of its high electron conductivity (4.1 × 10^{-7} S cm^{-1}) and deep LUMO level of −3.4 eV.[108,109] However, the EQE$_{max}$ was as low as 2.39%, which is lower than TPBi used device (5.11%), because the excess electrons flow as leakage current without radiative recombination, and charge imbalance promotes Auger nonradiative recombination.[108] The coevaporated B3PYMPM and TPBi reduced the amount of electron injection, and thereby charge balance is matched. Finally, high EQE$_{max}$ of 12.9% is obtained at the ratio of TPBi:B3PYMPM (2:1 w/w) (**Figure 9**a).[108]

Multilayer ETL using tris(8-hydroxyquinoline)aluminum(III) (Alq₃; μ_e = 1.4 × 10^{-6} cm^2 V^{-1} s^{-1}), TPBi (μ_e = 3.3 × 10^{-5} cm^2 V^{-1} s^{-1}) have been introduced for PeLEDs.[110] Even though Alq₃ has the most similar μ_e to hole transport material, PVK (1.0 × 10^{-6} cm^2 V^{-1} s^{-1}),[111] the EQE$_{max}$ was only 0.73%, which is lower than the TPBi based PeLED (EQE$_{max}$ = 0.75%).[110] The reason for the low EQE$_{max}$ is that Alq₃ has a shallow HOMO level and low bandgap, so holes and excitons cannot be confined in the EML.[110] Leaked holes flowed and recombined in the Alq₃ layer and make a broad electroluminescence spectrum.[110] In contrast, the TPBi-based device showed a single emission peak from MHP; this result indicates effective hole and exciton confinement.[110] TPBi (15 nm)/Alq₃ (10 nm)/TPBi
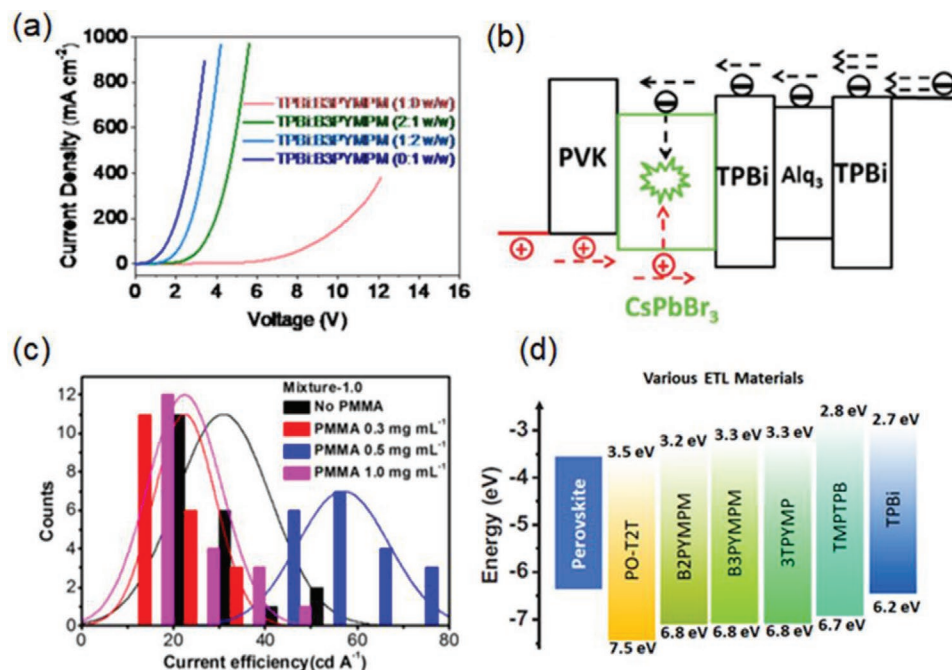

Figure 9. ETLs for highly efficient PeLEDs. a) Current density depends on the ratio of TPBi and B3PYMPM. Reproduced with permission.[108] Copyright 2018, American Chemical Society. b) Electron injection control using the sandwiched Alq₃ layer. Reproduced with permission.[110] Copyright 2018, Wiley-VCH. c) Current efficiency by tuning the PMMA thickness. Reproduced with permission.[22] Copyright 2018, Nature Publishing Group. d) Energy band diagram of the various ETL materials.

**ADVANCED
SCIENCE NEWS**

www.advancedsciencenews.com

**ADVANCED
MATERIALS
INTERFACES**

www.advmatinterfaces.de

(10 nm) sandwiched structure is suggested to obtain a precise charge balance.[110] An additional Alq_3 layer between TPBi layers decrease the electron injection by its low μ_e while the thin TPBi layer between MHP and Alq_3 blocks hole leakage current.[110] This structure had $EQE_{max} = 1.43\%$, i.e., double that of the conventional TPBi device (Figure 9b).[110]

4.1.2. Insulating Interlayer for Charge Balance

A thin layer of insulating material between EML and ETL can decrease electron injection. In a PEDOT:PSS/MA-CsPbBr$_3$ film/ B3PYMPM/LiF/Al structure, a thin layer of poly(methyl methacrylate) (PMMA) is deposited between the EML and the ETL.[22] This layer decreased electron injection and improved charge balance, therefore yielded $EQE_{max} = 20.3\%$, which is higher than $EQE_{max} = 17\%$ without the PMMA layer (Figure 9c).[22]

Polyethylenimine ethoxylated (PEIE) is also introduced as a thin insulating layer to achieve charge balance.[112] The insulating PEIE layer decreased electron injection from high-μ_e material Bathophenanthroline (Bphen), and thereby matched charge balance, and also protected the MHP layer from oxygen and moisture. As a result, efficiency and stability were both increased.[112]

4.1.3. Hole Blocking with Deep HOMO Level

Electron transport materials with deep HOMO level can act as a hole-blocking layer (HBL) which can confine holes in the EML.[113] Effective confinement of exciton is especially essential in blue-emitting PeLEDs due to their deep HOMO level of the EML. Therefore, B3PYMPM,[106] B2PYMPM,[43] 3TPYMB,[43,114] TmPyPB,[114] PO-T2T[107] which have deep HOMO level, have been used to obtain efficient blue-emitting PeLEDs (Figure 9d). Replacement of TPBi with PO-T2T (HOMO = −7.5 eV, $\mu_e = 1.1 \times 10^{-4}$ cm^2 V^{-1} s^{-1})[115] improved charge balance and hole confinement, and therefore increased EQE_{max} by 1.36 times to 1.96% at 477 nm.[107] Also, an additional thin layer (≈15 nm) of B2PYMPM or 3TPYMB has been introduced as an HBL between the TPBi (≈45 nm) ETL and EML.[43] Use of B2PYMPM slightly decreased the current density and luminance, but increased EQE_{max} to 2.25% in blue PeLEDs; this result means that hole confinement and charge balance were improved.[43]

4.2. Electron Injection Layer(EIL) and WF Control

Efficient electron injection requires sufficiently small energy barrier between the metal cathode and the EML. The LUMO levels of typical organic ETL materials are from −2 to −3 eV compared to the vacuum level, therefore metal with low WF such as Mg (3.66 eV), Ca (2.87 eV), are candidates for efficient electron injection to ETL from the electrode.[116] However, metals that have low WF are highly reactive that easily oxidized in ambient conditions. To reduce WF of the less-reactive cathode such as Al (4.28 eV) and Ag (4.26 eV) , a metal fluoride interlayer can be inserted as an EIL. LiF/Al structure, which has a low WF of 2.7 eV, has been widely used,[116] and high effi-

cient PeLEDs works are reported with LiF/Al cathode.[22,56,103] Meanwhile, although LiF layer is an efficient EIL layer, several disadvantages have remained. For LiF, only a few materials of Al, Mg, Ca can be used for the metal electrode which can react with LiF.[117] Also, very precise thickness control in the range of 0.1–5 nm is needed for LiF, because only a small difference of thickness can largely change the electron injection.[118] Furthermore, lithium species which are decomposed from LiF during thermal deposition can diffuse into the device, and decrease the fluorescence yield of EML.[119–121]

Low WF metal, Ytterbium (Yb, WF = 2.6 eV),[120] was introduced as alternative EIL material under Ag cathode. This Yb/ Ag (WF = 2.6 eV) structure can inject electrons into the TPBi ($E_{LUMO} = -2.7$ eV) freely without a barrier, and therefore prevent accumulation of space charges which could degrade the efficiency and lifetime of PeLEDs.[120] Compared to other EIL/ cathode structures, such as Liq/Al (WF = 2.9 eV), Mg/Ag (WF = 3.7 eV) and Ag (WF = 4.3 eV), barrier-free Yb/Ag (WF = 2.6 eV) achieved the best device efficiency of $L_{max.} = 19\,160$ cd m^{-2}, $EQE_{max} = 5.28\%$ and the lowest V_{on} of 3.0 V.[121] Furthermore, the thickness of Yb (≈2, 5, 10 nm) does not affect the device performance, because Yb is low WF metal itself.[121]

Although Yb can act as efficient barrier-free EIL and exhibit thickness independent properties, Yb is a low WF metal that is highly reactive and limit the device lifetime. As both LiF and Yb have obvious limitations, new types of EIL materials are required, which can satisfy the following abilities: The ideal EILs need to i) sufficiently decrease the effective WF of metal electrodes such as Al and Ag and facilitate the electron injection, ii) exhibit thickness independent property, and iii) be less reactive with other organic layers. Otherwise, metal oxides can be a good alternative for ETL, which does not need an EIL due to their deep CBM level.

4.3. Metal Oxide for ETL

Metal oxide semiconductors present promising candidates for use as an ETL because of their excellent chemical stability, low cost, and compatibility with solution processing. Therefore, metal oxide NPs such as ZnO and their derivatives (e.g., ZnMgO) are commonly used for ETL in the quantum dot LEDs (QLEDs).[122,123] However, organic ETL materials are more widely used rather than metal oxides in PeLEDs.

This difference between QLEDs and PeLEDs mainly arises from the bandgap alignment of the EML and the ETL. cQDs have deeper valence band maximum (VBM) levels and CBM levels than organic light-emitting materials and MHPs.[111,124–126] Metal oxides ETLs also exhibit deep CBM level. Because of their deep aligning band structure, CBM levels of cQDs (−3.5–4.5 eV), metal oxides ETL (ZnO ≈ 4.0 eV), and the WF of the metal cathode(Ag = 4.6 eV Ag, Al = 4.1 eV for Al) are very close, and only very small electron injection barrier exists. Thus, metal oxides are a suitable candidate for ETL materials of QLEDs because of their adequate CBM levels (−3–4 eV).[127]

Meanwhile, MHP have more shallow CBM levels (−3.3–4.0 eV). The deep aligning CBM of the metal oxides acts as a barrier that can impede electron injection. Also, electrons can be transferred spontaneously from the MHP layer to the metal oxide at the interface. Excitons easily dissociated at the
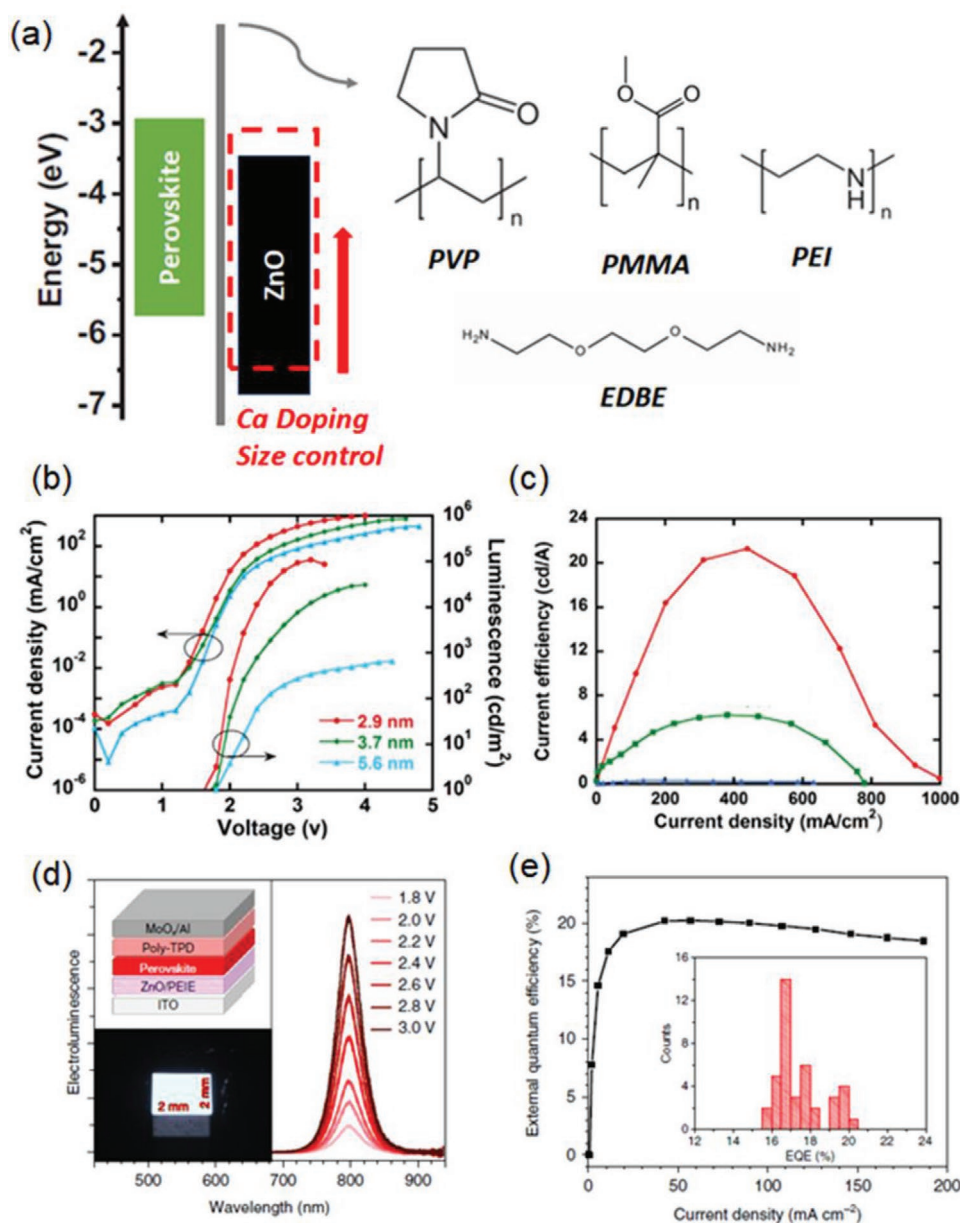
Figure 10. a) Energy diagram of perovskite and ZnO NP layer, and candidates for interlayer on ZnO. b) Current density, luminescence, and c) current efficiency plot based on the size of the ZnO NP. Reproduced with permission.[133] Copyright 2018, Wiley-VCH. d) Device structure, EL spectrum, a photograph, and e) EQE versus current density plot of PeLEDs with an inverted structure based on ZnO/PEIE ETL. inset: EQE histograms of PeLEDs. Reproduced with permission.[136] Copyright 2019, Nature Publishing Group.

MHP/metal oxide interface due to the electron transfer from the MHP to the metal oxide which results in the positively charged MHP, and decrease of device efficiency.[128] The incorporation of an interlayer or modulating metal oxide materials at the interface has been conducted to solve those problems (**Figure 10**a).

4.3.1. Increasing CBM of ZnO NPs

Doping or reducing the size of ZnO NPs can increase the CBM and improve the efficiency of PeLEDs. Ca-doped ZnO (CZO) NPs can be used to overcome the deep-lying CBM of

ZnO NPs to increase electron injection.[129] Doping with 50% Ca increased the CBM from −4.07 to −3.07 eV and μ_e from 2.4 × 10^{-3} to 5.7 × 10^{-2} cm^2 V^{-1} s^{-1}.[129] PL quenching at the MHP/CZO interface is reduced, because the charge transfer from MHP to CZO is suppressed.[129] The devices showed significantly improved EQE$_{max}$ = 5.8% for red emission at 634 nm and 6.2% for green emission at 540 nm.[129] Doping of ZnO with Mg (ZnMgO) also raised the CBM of ZnMgO NPs to −3.85 eV.[130] N-butylammonium bromide and polyethylene oxide are mixed in the MHP precursor to avoid degradation of MHP from the 2-propanol used for the solvent of ZnMgO NPs.[131] The device with conventional all-inorganic ITO/NiO$_x$/CsPbBr$_3$

ADVANCED
SCIENCE NEWS
www.advancedsciencenews.com

ADVANCED
MATERIALS
INTERFACES
www.advmatinterfaces.de

film/ZnMgO/Al structure showed CE_{max} = 2.97 cd A^{-1}, L_{max} of 14,521 cd m^{-2}, and half-lifetime of 216 min at constant 3 V without encapsulation.[130]

The CBM level and μ_e could be increased by decreasing the size of the ZnO NP.[132] In ITO/PEDOT:PSS/PC FAPbBr$_3$/ZnO/Ag structure, electrons are minority carriers because of the high electron-injection barrier from the 5.6 nm ZnO CBM = −4.14 eV to the CBM level = −3.57 eV of PC FAPbBr$_3$ film.[133] Decreasing the ZnO NP size to 2.9 nm can reduce the electron-injection barrier from ZnO to FaPbBr$_3$ film by increasing the CBM level to −3.94 eV.[133] 2.9 nm ZnO NP yielded EQE_{max} = 4.66% and L_{max} = 10 900 cd m^{-2}, whereas 5.6 nm NPs yielded EQE_{max} = 0.35% and L_{max} = 1070 cd m^{-2} (Figure 10b,c).[133]

4.3.2. Reducing the Interface Quenching on Metal Oxide

An additional interlayer between ZnO and MHP can reduce the interface quenching. First, an insulating layer (e.g., PVP and PMMA) between ZnO and MHP layer was introduced. The PVP layer increased the PL lifetime of MHP, and the five times increased the PL intensity of CsPbBr$_3$ was achieved.[65] This result indicates that PVP passivates defects and suppresses the exciton quenching at the MHP and ZnO interface. The hydrophilic PVP layer also improved the wetting of the MHP precursor, so the film coverage of the MHP film increased and the number of pinholes was reduced.[65] PeLED that had the PVP layer showed lower leakage current and improved device efficiency of EQE_{max} = 10.43%.[65] Similarly, use of a thin PMMA layer between the EML and the ZnO ETL increased the PL intensity by reducing quenching sites between ZnO and MHP.[134] Also, the PMMA layer can decrease the leakage current and increase the efficiency of PeLEDs. However, PMMA is an insulator, so at thickness >10 nm, an electron-injection barrier formed and thus reduced both EQE_{max} and L_{max}.[134] Those insulating polymers with low dielectric constant can provide both a charge-blocking and buffer layer between MHP and ZnO which can make better charge balance and suppress the interfacial quenching. But those materials showed a limitation that can interrupt the electron injection and increase the V_{on}, which also lowered the device lifetime.[65,134]

Amine group rich material such as polyethyleneimine (PEI)[128,135] PEIE,[23,136] and 2,2-(ethylenedioxy) bis(ethylammonium) (EDBE)[137] not only suppress the exciton quenching, but also induce strong molecular dipoles and cause a reduction of CBM of ZnO.[138] When the PEI is deposited on the ZnO layer, CBM of ZnO is reduced by 0.44 eV, and can thereby increase electron injection. Also, it can prevent spontaneous charge transfer, which leads to an increase of PLQY from 15% to 70%.[128] Optimized PEI layer thickness yielded EQE_{max} = 6.30% and L_{max} = 2,216 cd m^{-2}.[128] When PEIE was also used as a surface modifier of ZnO NPs, with properly aligned HTL of poly-TPD for better charge balance, infrared-emitting FAPbI$_3$ PeLED reached 20.2% EQE_{max} (Figure 10d,e).[136] Similarly, overcoating of hydrophilic EDBE on ZnMgO NPs can passivate the defects of the MHP, and thereby increase PL intensity.[137] Additionally, the device with EDBE had higher current density and V_{on} was lowered from 2.0 to 1.5 V compared to the device without EDBE.[137] This result indicates improved electron injection, possibly because of the interface dipole from the EDBE to ZnMgO NPs layer.[137] In a near-infrared PeLED, the EDBE interlayer on ZnMgO NPs improved EQE_{max} from 9.15% to 12.35%.[137]

5. Insulator/MHP/Insulator Structure

PC MHPs have long PL lifetime (≈50 ns) and exciton diffusion length,[10] whereas charge-separation time at interface between EML and HTL or ETL is about 1 ns; as a result, they are vulnerable to PL quenching.[139] Also, typically PC MHPs crystallize quickly, so nonuniform film with pinholes forms and thus cause a leakage current, which can degrade device efficiency.[44] Insulator/MHP/Insulator (IPI) structure has been suggested as a way to avoid this degradation.

IPI structure exploits metal-insulator/semiconductor (MIS) contact.[139,140] A thin insulating LiF layer is inserted between the ITO and MHP layer, without any HIL/HTL. The LiF has a large hole injection barrier, but holes can be injected by tunneling.[141] During the operation, charge carriers and ions accumulate at the MHP/LiF interface. This process leads to a large drop in potential at the insulating layer, and consequently this drop can reduce the tunneling distance from ITO to the MHP layer.[48] A thin (4 nm) LiF layer is deposited between ITO and EML, and a thick (8 nm) LiF layer and Bphen are used together as the ETL.[142] Additional LiF interlayers efficiently suppress PL quenching at interfaces between MHP and ITO or ETL. This structure can also suppress leakage currents. In the conventional LED structure, the HTL can be connected with the ETL directly through pinholes in the EML, and current can traverse through this connection as a non-radiative path.[142] When LiF is deposited at the both sides of the MHP layer, charges cannot bypass through pinhole region because both the LiF layers merged together to make a thick film beyond charge tunneling thickness. Therefore, the charges can tunnel instead through the MHP region because a separate LiF layer on the top or on the bottom of the MHP layer is still within a tunneling regime (**Figure 11**a).[140] IPI structure increased device efficiency by 30 times in devices that used FAPbBr$_3$, and increased half-lifetime at 100 cd m^{-2} from 4 to 96 h in devices that used CsPbBr$_3$.[142]

Meanwhile, all inorganic IPI structure showed remarkable device stability for PeLEDs. Thin LiF interlayers are used for insulating layers as described above, and additionally inorganic ZnS and ZnSe are deposited for ETL instead of organic ETL electron transport materials (Figure 11b).[143] The device exhibited extremely long half-lifetime of 255 h at 120 cd m^{-2}, L_{max} of 156 155 cd m^{-2}, and EQE_{max} of 11.05% (Figure 11c).[143] The reason for the long device lifetime is confirmed by elemental analysis. The inorganic ETL and IPI structured device retained the elements of MHP after 50 min operation, while a large number of elements of MHP were diffused through interlayers in the conventional structured device.[143] Compact inorganic ETLs and insulating LiF interlayers can sufficiently block the ion migration.[143]

6. Conclusion

In this review, we have stressed some strategies of interfacial engineering to improve the efficiency of PeLEDs focusing on

**ADVANCED
SCIENCE NEWS**
www.advancedsciencenews.com

**ADVANCED
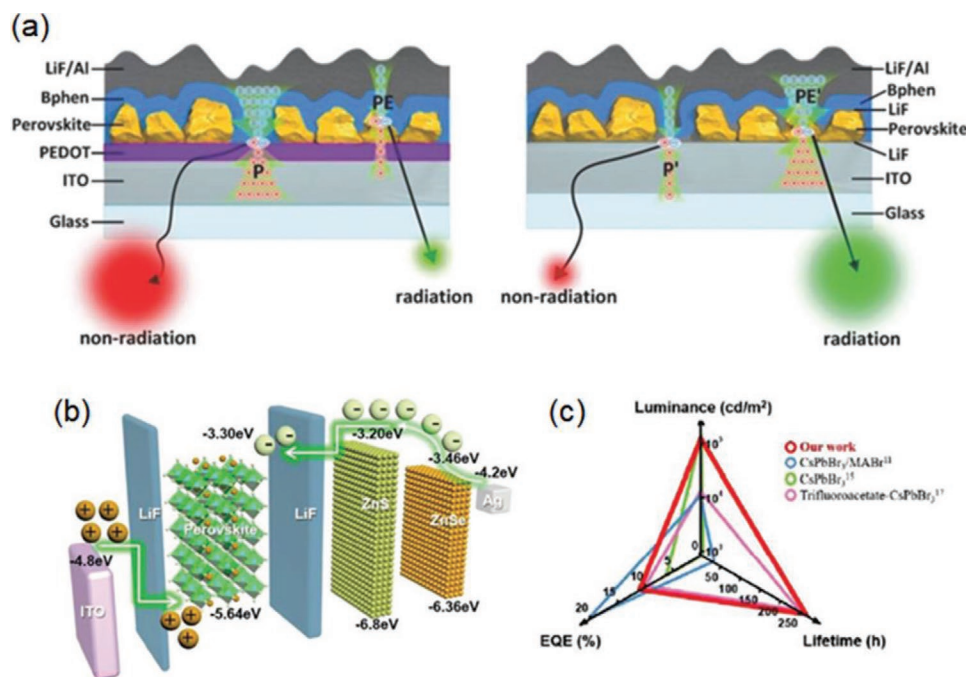MATERIALS
INTERFACES**
www.advmatinterfaces.de

Figure 11. a) Schematic illustration of the working mechanism of conventional PeLEDs (left) and IPI structure-based PeLEDs (right). Current mainly leaked through the gap of perovskite in conventional PeLEDs, while reverse tendency was showed in IPI structure-based PeLEDs. Reproduced with permission.[140] Copyright 2018, Wiley-VCH. b) Schematic band structure of IPI structure-based all inorganic PeLEDs. c) EL performance of reported PeLEDs. Reproduced with permission.[143] Copyright 2020, Wiley-VCH.

several aspects: i) Adequate band alignment to reduce injection energy barrier and boost the charge injection, ii) charge blocking to reduce the leakage current and confine exciton in MHP layer, iii) Surface energy tailoring for smooth MHP layer, and iv) Passivation of surface defects to decrease exciton quenching. Suggested strategies can be generally applicable for all PeLEDs and will give an insight to further increase the efficiency of PeLEDs. Moreover, we also introduced PeLEDs with recently reported new interfacial layer materials (e.g., black phosphorous,[62] cuprous oxide[64]) or a new charge injection/blocking structure (e.g., insulator/perovskite/insulator[139,141]), which expands the applicability of PeLEDs.

In a short period, PeLEDs have achieved such a high EQE over 20% for the infrared,[24,136] red,[20,25] green-emitting[23] devices and 12% for blue-emitting devices.[11] Such rapid development in PeLEDs is a result of the synergistic effects between MHP EML engineering and device architecture designing. Despite the fast evolution of PeLED efficiency, several problems are remaining. Also, the relatively low EQE for the deep blue-emitting PeLEDs is a major task to be overcome shortly. Last, PeLEDs critically suffer from low stability compared to conventional OLED or QLED might be attributed to ion migration of MHP.

We anticipate that our review would offer insight to overcome the above-mentioned unresolved issues. Interlayers with deep-lying HOMO levels atop a conventional HIL/HTL can be effective to achieve a decline in energy offset at the interface[54] and further precise design for efficient hole injection will increase the efficiency in PeLEDs: this approach will be also very effective in blue emitting PeLEDs that have a MHP EML with deep VBM. Increasing the stability of PeLEDs is a more difficult task[144] because more complicated and delicate

approaches should be combined. On top of the previously suggested degradation mechanism,[144] this review paper suggests that the lifetime can be also enhanced by defect passivation layer. Passivating agent in a defect passivation layer should effectively penetrate into a MHP layer to effectively passivate defects at the surface of nanograins and grain boundaries in PC MHPs or surface defects in colloidal PeNPs.[29] Reduced defect sites can significantly reduce the ion-migration which can accelerate the device abrupt failure. Reducing the charge accumulation at the interface and reaction with redox-active PEDOT:PSS and reactive cathodes by engineering device architecture can also be effective strategies to enhance the device stability.

For high brightness applications, efficiency roll-off at high current density is another vital task to overcome. There are few possible origins of efficiency roll-off in PeLED such as unbalanced charge injection, Joule heating, and Auger recombination.[36,145,146] Internal QY of MHP critically decreases as the temperature increases due to thermal energy-induced exciton dissociation. Therefore, heat generation at the high current density should be minimized while the charges are injected; the charge injection layer requires high conductivity without an injection barrier to reduce the series resistance of PeLED which is responsible for Joule heating and to boost the balanced charge injection.

It is still controversial that the Auger recombination is responsible for the efficiency roll-off of PeLED. Zou and co-workers[36] claimed that the Auger recombination is a major reason for efficiency roll-off, while Kim and co-workers[145] claimed unbalanced charge injection and Joule heating is the dominant reason for EQE roll-off rather than Auger recombination. Auger recombination might be more critical for smaller

**ADVANCED
SCIENCE NEWS**

www.advancedsciencenews.com

**ADVANCED
MATERIALS
INTERFACES**

www.advmatinterfaces.de

MHP crystals in nano dimension because they have higher carrier localization in MHP nanocrystals.[36] To reduce the Auger recombination in reduced dimension, spacer which can delocalize exciton, i.e., thick shell in MHP NP as in traditional cQD, will be effective to minimize the efficiency roll-off.[147] Auger recombination in MHP with various dimensions and structure needs to be further studied.

Therefore, charge injection, transport and recombination dynamics must be further comprehensively studied. Under the understanding of the behavior of charges in PeLEDs, device engineering for efficient and stable PeLEDs will be enabled. In addition, a standard of consensus for the composition of perovskites and interlayer materials should be determined according to the targeted energy levels of the devices.

Acknowledgements

Conflict of Interest

The authors declare no conflict of interest.

Keywords

[1] H. Ren, S. Yu, L. Chao, Y. Xia, Y. Sun, S. Zuo, F. Li, T. Niu, Y. Yang, H. Ju, B. Li, H. Du, X. Gao, J. Zhang, J. Wang, L. Zhang, Y. Chen, W. Huang, *Nat. Photonics* **2020**, *14*, 154.

[2] K.-G. Lim, S. G. Ji, J. Y. Kim, T.-W. Lee, *Small Methods* **2020**, *4*, 2000065.

[3] Q. Shang, M. Li, L. Zhao, D. Chen, S. Zhang, S. Chen, P. Gao, C. Shen, J. Xing, G. Xing, B. Shen, X. Liu, Q. Zhang, *Nano Lett.* **2020**, *9*, 6636.

[4] M. Stylianakis, T. Maksudov, A. Panagiotopoulos, G. Kakavelakis, K. Petridis, *Materials* **2019**, *12*, 859.

[5] H. Sun, W. Tian, F. Cao, J. Xiong, L. Li, *Adv. Mater.* **2018**, *30*, 1706986.

[6] L. Dou, Y. (.M.). Yang, J. You, Z. Hong, W.-H. Chang, G. Li, Y. Yang, *Nat. Commun.* **2014**, *5*, 5404.

[7] M.-H. Park, J. S. Kim, J.-M. Heo, S. Ahn, S.-H. Jeong, T.-W. Lee, *ACS Energy Lett.* **2019**, *4*, 1134.

[8] Z.-K. Tan, R. S. Moghaddam, M. L. Lai, P. Docampo, R. Higler, F. Deschler, M. Price, A. Sadhanala, L. M. Pazos, D. Credgington, F. Hanusch, T. Bein, H. J. Snaith, R. H. Friend, *Nat. Nanotechnol.* **2014**, *9*, 687.

[9] Y.-H. Kim, H. Cho, J. H. Heo, T.-S. Kim, N. Myoung, C.-L. Lee, S. H. Im, T.-W. Lee, *Adv. Mater.* **2015**, *27*, 1248.

[10] H. Cho, S.-H. Jeong, M.-H. Park, Y.-H. Kim, C. Wolf, C.-L. Lee, J. H. Heo, A. Sadhanala, N. Myoung, S. Yoo, S. H. Im, R. H. Friend, T.-W. Lee, *Science* **2015**, *350*, 1222.

[11] Y. Dong, Y.-K. Wang, F. Yuan, A. Johnston, Y. Liu, D. Ma, M.-J. Choi, B. Chen, M. Chekini, S.-W. Baek, L. K. Sagar, J. Fan, U. Hou, M. Wu, S. Lee, B. Sun, S. Hoogland, R. Quintero-Bremudez, H. Ebe, P. Todorovic, F. Dinic, P. Li, H. T. Kung, M. I. Saidaminov, E. Kumacheva, E. Spiecker, L.-S. Liao, O. Voznyy, Z.-H. Lu, E. H. Sargent, *Nat. Nanotechnol.* **2020**, *15*, 668.

[12] K. X Steirer, P. Schulz, G. Teeter, V. Stevanovic, M. Yang, K. Zhu, J. J. Berry, *ACS Energy Lett.* **2016**, *1*, 360.

[13] J. Kang, L.-W. Wang, *J. Phys. Chem. Lett.* **2017**, *8*, 489.

[14] H. M. Jang, J.-S. Kim, J.-M. Heo, T.-W. Lee, *APL Mater.* **2020**, *8*, 020904.

[15] Y.-H. Kim, C. Wolf, Y. Kim, H. Cho, W. Kwon, A. Sadhanala, C. G. Park, S. Rhee, S. H. Im, H. Richard, T.-W. Lee, *ACS Nano* **2017**, *11*, 6586.

[16] Y.-H. Kim, H. Cho, T.-W. Lee, *Proc. Natl. Acad. Sci. USA* **2016**, *113*, 11694.

[17] D. Zhang, Y. Yang, Y. Bekenstein, Y. Yu, N. A. Gibson, A. B. Wong, S. W. Eaton, N. Kornienko, Q. Kong, M. Lai, A. P Alivisatos, S. R. Leone, P. Yang, *J. Am. Chem. Soc.* **2016**, *138*, 7236.

[18] G. Nedelcu, L. Protesescu, S. Yakunin, M. I. Bodnarchuk, M. J. Grotevent, M. V. Kovalenko, *Nano Lett.* **2015**, *15*, 5635.

[19] R. Prasanna, A. Gold-Parker, T. Leijtens, B. Conings, A. Babayigit, H.-G. Boyen, M. F. Toney, M. D. Mcgehee, *J. Am. Chem. Soc.* **2017**, *139*, 11117.

[20] T. Chiba, Y. Hayashi, H. Ebe, K. Hoshi, J. Sato, S. Sato, Y.-J. Pu, S. Ohisa, J. Kido, *Nat. Photonics* **2018**, *12*, 681.

[21] X. Zhao, Z.-K. Tan, *Nat. Photonics* **2020**, *14*, 215.

[22] K. Lin, J. Xing, L. N. Quan, F. P. G. de Arquer, X. Gong, J. Lu, L. Xie, W. Zhao, D. Zhang, C. Yan, W. Li, X. Liu, Y. Lu, J. Kirman, E. H. Sargent, Q. Xiong, Z. Wei, *Nature* **2018**, *562*, 245.

[23] W. Xu, Q. Hu, S. Bai, C. Bao, Y. Miao, Z. Yuan, T. Borzda, A. J. Barker, E. Tyukalova, Z. Hu, M. Kawecki, H. Wang, Z. Yan, X. Liu, X. Shi, K. Uvdal, M. Fahlman, W. Zhang, M. Duchamp, J.-M. Liu, A. Petrozza, J. Wang, L.-M. Liu, W. Huang, F. Gao, *Nat. Photonics* **2019**, *13*, 418.

[24] B. Zhao, S. Bai, V. Kim, R. Lamboll, R. Shivanna, F. Auras, J. M. Richter, L. Yang, L. Dai, M. Alsari, X. J. She, L. Liang, J. Zhang, S. Lilliu, P. Gao, H. J. Snaith, J. Wang, N. C. Greenham, R. H. Friend, D. Di, *Nat. Photonics* **2018**, *12*, 783.

[25] Y. Cao, N. Wang, H. Tian, J. Guo, Y. Wei, H. Chen, Y. Miao, W. Zou, K. Pan, Y. He, H. Cao, Y. Ke, M. Xu, Y. Wang, M. Yang, K. Du, Z. Fu, D. Kong, D. Dai, Y. Jin, G. Li, H. Li, Q. Peng, J. Wang, W. Huang, *Nature* **2018**, *562*, 249.

[26] Y.-H. Kim, C. Wolf, H. Kim, T.-W. Lee, *Nano Energy* **2018**, *52*, 329.

[27] M.-H. Park, J. Park, J. Lee, H. S. So, H. Kim, S.-H. Jeong, T.-H. Han, C. Wolf, H. Lee, S. Yoo, T.-W. Lee, *Adv. Funct. Mater.* **2019**, *29*, 1902017.

[28] M.-H. Park, S.-H. Jeong, H.-K. Seo, C. Wolf, Y.-H. Kim, H. Kim, J. Byun, J. S. Kim, H. Cho, T.-W. Lee, *Nano Energy* **2017**, *42*, 157.

[29] C. Quan, Q. Du, M. Li, R. Wang, Q. Ouyang, S. Su, S. Zhu, Q. Chen, Y. Sheng, L. Chen, H. Wang, D. G. Campbell, C. Mackintosh, Z. Yang, K. Ouyang, H. Y. Wang, S. Chen, *Nat. Commun.* **2020**, *11*, 2186.

[30] J. Byun, H. Cho, C. Wolf, M. Jang, A. Sadhanala, R. H. Friend, H. Yang, T.-W. Lee, *Adv. Mater.* **2016**, *28*, 7515.

[31] Y.-H. Kim, G.-H. Lee, Y.-T. Kim, C. Wolf, H. J. Yun, W. Kwon, C. G. Park, T.-W. Lee, *Nano Energy* **2017**, *38*, 51.

[32] L. Protesescu, S. Yakunin, M. I. Bodnarchuk, F. Krieg, R. Caputo, C. H. Hendon, R. X. Yang, A. Walsh, M. V. Kovalenko, *Nano Lett.* **2015**, *15*, 3692.

[33] J. Park, H. M. Jang, S. Kim, S. H. Jo, T.-W. Lee, *Trends Chem.* **2020**, *2*, 837.

[34] F. Zhang, H. Zhong, C. Chen, X.-G. Wu, X. Hu, H. Huang, J. Han, B. Zou, Y. Dong, *ACS Nano* **2015**, *9*, 4533.

[35] G. Xing, B. Wu, X. Wu, M. Li, B. Du, Q. Wei, J. Guo, E. K. L. Yeow, T. C. Sum, W. Huang, *Nat. Commun.* **2017**, *8*, 14558.

[36] W. Zou, R. Li, S. Zhang, Y. Liu, N. Wang, Y. Cao, Y. Miao, M. Xu, Q. Guo, D. Di, L. Zhang, C. Yi, F. Gao, R. H. Friend, J. Wang, W. Huang, *Nat. Commun.* **2018**, *9*, 608.

[37] A. Fakharuddin, W. Qiu, G. Croes, A. Devižis, R. Gegevičius, A. Vakhnin, C. Rolin, J. Genoe, R. Gehlhaar, A. Kadashchuk, V. Gulbinas, P. Heremans, *Adv. Funct. Mater.* **2019**, *29*, 1904101.

[38] S.-H. Jeong, J. Park, T.-H. Han, F. Zhang, K. Zhu, J. S. Kim, M.-H. Park, M. O. Reese, S. Yoo, T.-W. Lee, *Joule* **2020**, *7*, 1004.

[39] Y. Yang, C. Liu, Y. Ding, Z. Arain, S. Wang, X. Liu, T. Hayat, A. Alsaedi, S. Dai, *ACS Appl. Mater. Interfaces* **2019**, *11*, 34964.

[40] C. Li, N. Wang, A. Guerrero, Y. Zhong, H. Long, Y. Miao, J. Bisquert, J. Wang, S. Huettner, *J. Phys. Chem. Lett.* **2019**, *10*, 6857.

[41] S. Feldmann, S. Macpherson, S. P. Senanayak, M. Abdi-Jalebi, J. P. H. Rivett, G. Nan, G. D. Tainter, T. A. S. Doherty, K. Frohna, E. Ringe, R. H. Friend, H. Sirringhaus, M. Saliba, D. Beljonne, S. D. Stranks, F. Deschler, *Nat. Photonics* **2020**, *14*, 123.

[42] H.-S. Kim, I. Mora-Sero, V. Gonzalez-Pedro, F. Fabregat-Santiago, E. J. Juarez-Perez, N.-G. Park, J. Bisquert, *Nat. Commun.* **2013**, *4*, 2242.

[43] Y. Shynkarenko, M. I. Bodnarchuk, C. Bernasconi, Y. Berezovska, V. Verteletskyi, S. T. Ochsenbein, M. V Kovalenko, *ACS Energy Lett.* **2019**, *4*, 2703.

[44] S. Ahn, M.-H. Park, S.-H. Jeong, Y.-H. Kim, J. Park, S. Kim, H. Kim, H. Cho, C. Wolf, M. Pei, H. Yang, T.-W. Lee, *Adv. Funct. Mater.* **2018**, *1*, 1807535.

[45] H.-K. Seo, H. Kim, J. Lee, M.-H. Park, S.-H. Jeong, Y.-H. Kim, S.-J. Kwon, T.-H. Han, S. Yoo, T.-W. Lee, *Adv. Mater.* **2017**, *29*, 1605587.

[46] S. Lee, D. B. Kim, I. Hamilton, M. Daboczi, Y. S. Nam, B. R. Lee, B. Zhao, C. H. Jang, R. H. Friend, J.-S. Kim, M. H. Song, *Adv. Sci.* **2018**, *5*, 1801350.

[47] Z. Xiao, R. A. Kerner, N. Tran, L. Zhao, G. D. Scholes, B. P. Rand, *Adv. Funct. Mater.* **2019**, *29*, 1807284.

[48] C. Mai, D. Yu, J. Li, G. Huang, H. Zheng, L. Mu, J. Cun, J. Wang, G. Xie, J. Wang, J. Peng, Y. Cao, *Adv. Opt. Mater.* **2020**, *8*, 1902177.

[49] C. Bi, Q. Wang, Y. Shao, Y. Yuan, Z. Xiao, J. Huang, *Nat. Commun.* **2015**, *6*, 7747.

[50] Y. Li, B. Ding, Q. Q. Chu, G. J. Yang, M. Wang, C. X. Li, C. J. Li, *Sci. Rep.* **2017**, *7*, 46141.

[51] M. P. D. Jong, L. J. V. Ijzendoorn, M. J. A. D. Voigt, *Appl. Phys. Lett.* **2002**, *77*, 2255.

[52] M. K. Gangishetty, S. Hou, Q. Quan, D. N. Congreve, *Adv. Mater.* **2018**, *30*, e1706226.

[53] Z. Ren, X. Xiao, R. Ma, H. Lin, K. Wang, X. W. Sun, W. C. H. Choy, *Adv. Funct. Mater.* **2019**, *29*, 1904684.

[54] R. L. Z. Hoye, M.-L. Lai, M. Anaya, Y. Tong, K. Gałkowski, T. Doherty, W. Li, T. N. Huq, S. Mackowski, L. Polavarapu, J. Feldmann, J. L. Macmanus-Driscoll, R. H. Friend, A. S. Urban, S. D. Stranks, *ACS Energy Lett.* **2019**, *4*, 1181.

[55] L. Groenendaal, F. Jonas, D. Freitag, H. Pielartzik, J. R. Reynolds, *Adv. Mater.* **2000**, *12*, 481.

[56] J. Song, T. Fang, J. Li, L. Xu, F. Zhang, B. Han, Q. Shan, H. Zeng, *Adv. Mater.* **2018**, *30*, 1805409.

[57] D. Han, M. Imran, M. Zhang, S. Chang, X.-G. Wu, X. Zhang, J. Tang, M. Wang, S. Ali, X. Li, G. Yu, J. Han, L. Wang, B. Zou, H. Zhong, *ACS Nano* **2018**, *12*, 8808.

[58] S. Yuan, Z.-K. Wang, M.-P. Zhuo, Q.-S. Tian, Y. Jin, L.-S. Liao, *ACS Nano* **2018**, *12*, 9541.

[59] C. Zou, Y. Liu, D. S. Ginger, L. Y. Lin, *ACS Nano* **2020**, *14*, 6076.

[60] D. Bin Kim, J. C. Yu, Y. S. Nam, D. W. Kim, E. D. Jung, S. Y. Lee, S. Lee, J. H. Park, A. Y. Lee, B. R. Lee, D. Di Nuzzo, R. H. Friend, M. H. Song, *J. Mater. Chem. C* **2016**, *4*, 8161.

[61] Y. Meng, M. Ahmadi, X. Wu, T. Xu, L. Xu, Z. Xiong, P. Chen, *Org. Electron.* **2019**, *64*, 47.

[62] A. G. Ricciardulli, S. Yang, N. B. Kotadiya, G.-J. A. H. Wetzelaer, X. Feng, P. W. M. Blom, *Adv. Electron. Mater.* **2019**, *5*, 1800687.

[63] Y. Zou, M. Ban, Y. Yang, S. Bai, C. Wu, Y. Han, T. Wu, Y. Tan, Q. Huang, X. Gao, T. Song, Q. Zhang, B. Sun, *ACS Appl. Mater. Interfaces* **2018**, *10*, 24320.

[64] R. Chakraborty, H. Bhunia, S. Chatterjee, A. J. Pal, *J. Solid State Chem.* **2020**, *281*, 121021.

[65] L. Zhang, X. Yang, Q. Jiang, P. Wang, Z. Yin, X. Zhang, H. Tan, Y. M. Yang, M. Wei, B. R. Sutherland, E. H. Sargent, J. You, *Nat. Commun.* **2017**, *8*, 15640.

[66] Y. Ahn, S. Lee, D.-H. Kwak, M. Kim, D. Y. Kim, J. Kim, Y. Park, M. C. Suh, *Appl. Surf. Sci.* **2020**, *507*, 145071.

[67] R. Li, L. Cai, Y. Zou, H. Xu, Y. Tan, Y. Wang, J. Li, X. Wang, Y. Li, Y. Qin, D. Liang, T. Song, B. Sun, *ACS Appl. Mater. Interfaces* **2020**, *12*, 36681.

[68] Z. Li, K. Cao, J. Li, X. Du, Y. Tang, B. Yu, *Org. Electron.* **2020**, *81*, 105675.

[69] S. T. Zhang, X. M. Ding, J. M. Zhao, H. Z. Shi, J. He, Z. H. Xiong, H. J. Ding, E. G. Obbard, Y. Q. Zhan, W. Huang, X. Y. Hou, *Appl. Phys. Lett.* **2004**, *84*, 425.

[70] K.-H. Wang, Y. Peng, J. Ge, S. Jiang, B.-S. Zhu, J. Yao, Y.-C. Yin, J.-N. Yang, Q. Zhang, H.-B. Yao, *ACS Photonics* **2019**, *6*, 667.

[71] X.-F. Peng, X.-Y. Wu, X.-X. Ji, J. Ren, Q. Wang, G.-Q. Li, X.-H. Yang, *J. Phys. Chem. Lett.* **2017**, *8*, 4691.

[72] T.-W. Lee, Y. Chung, *Adv. Funct. Mater.* **2008**, *18*, 2246.

[73] Y. Liu, T. Wu, Y. Liu, T. Song, B. Sun, *APL Mater.* **2019**, *7*, 021102.

[74] S.-H. Jeong, H. Kim, M.-H. Park, Y. Lee, N. Li, H.-K. Seo, T.-H. Han, S. Ahn, J.-M. Heo, K. S. Kim, T.-W. Lee, *Nano Energy* **2019**, *60*, 324.

[75] N. Kim, B. H. Lee, D. Choi, G. Kim, H. Kim, J. R. Kim, J. Lee, Y. H. Kahng, K. Lee, *Phys. Rev. Lett.* **2012**, *109*, 106405.

[76] L. Ouyang, C. Musumeci, M. J. Jafari, T. Ederth, O. Inganäs, *ACS Appl. Mater. Interfaces* **2015**, *7*, 19764.

[77] S.-S. Meng, Y.-Q. Li, J.-X. Tang, *Org. Electron.* **2018**, *61*, 351.

[78] J. Lu, W. Feng, G. Mei, J. Sun, C. Yan, D. Zhang, K. Lin, D. Wu, K. Wang, Z. Wei, *Adv. Sci.* **2020**, *7*, 2000689.

[79] Y. Shen, L.-P. Cheng, Y.-Q. Li, W. Li, J.-D. Chen, S.-T. Lee, J.-X. Tang, *Adv. Mater.* **2019**, *31*, 1901517.

[80] J. Kim, C.-H. Chung, K.-H. Hong, *Phys. Chem. Chem. Phys.* **2016**, *18*, 27143.

[81] H. Oga, A. Saeki, Y. Ogomi, S. Hayase, S. Seki, *J. Am. Chem. Soc.* **2014**, *136*, 13818.

[82] H.-B. Kim, H. Choi, J. Jeong, S. Kim, B. Walker, S. Song, J. Y. Kim, *Nanoscale* **2014**, *6*, 6679.

[83] X. Yang, X. Zhang, J. Deng, Z. Chu, Q. Jiang, J. Meng, P. Wang, L. Zhang, Z. Yin, J. You, *Nat. Commun.* **2018**, *9*, 2.

[84] W. Bi, X. Huang, Y. Tang, H. Liu, P. Jia, K. Yu, Y. Hu, Z. Lou, F. Teng, Y. Hou, *Org. Electron.* **2018**, *63*, 216.

[85] T. Zhao, C.-C. Chueh, Q. Chen, A. Rajagopal, A. K.-Y. Jen, *ACS Energy Lett.* **2016**, *1*, 757.

[86] W. Nie, J.-C. Blancon, A. J. Neukirch, K. Appavoo, H. Tsai, M. Chhowalla, M. A. Alam, M. Y. Sfeir, C. Katan, J. Even, S. Tretiak, J. J. Crochet, G. Gupta, A. D. Mohite, *Nat. Commun.* **2016**, *7*, 11574.

[87] W. Tress, M. Yavari, K. Domanski, P. Yadav, B. Niesen, J. P. Correa Baena, A. Hagfeldt, M. Graetzel, *Energy Environ. Sci.* **2018**, *11*, 151.

[88] D. Meggiolaro, E. Mosconi, F. De Angelis, *ACS Energy Lett.* **2019**, *4*, 779.

[89] Q. Jiang, Y. Zhao, X. Zhang, X. Yang, Y. Chen, Z. Chu, Q. Ye, X. Li, Z. Yin, J. You, *Nat. Photonics* **2019**, *13*, 460.

[90] X. Zheng, B. Chen, J. Dai, Y. Fang, Y. Bai, Y. Lin, H. Wei, X. C. Zeng, J. Huang, *Nat. Energy* **2017**, *2*, 17102.

[91] H.-S. Yoo, N.-G. Park, *Sol. Energy Mater. Sol. Cells* **2018**, *179*, 57.

[92] T. Tachikawa, I. Karimata, Y. Kobori, *J. Phys. Chem. Lett.* **2015**, *6*, 3195.

[93] D. W. De Quilettes, S. M. Vorpahl, S. D. Stranks, H. Nagaoka, G. E. Eperon, M. E. Ziffer, H. J. Snaith, D. S. Ginger, *Science* **2015**, *348*, 683.

[94] N. K. Noel, A. Abate, S. D. Stranks, E. S. Parrott, V. M. Burlakov, A. Goriely, H. J. Snaith, *ACS Nano* **2014**, *8*, 9815.

[95] W.-S. Shen, S. Yuan, Q.-S. Tian, Y.-C. Tao, Q. Wang, L.-S. Liao, *J. Mater. Chem. C* **2019**, *7*, 14725.

[96] A. Abate, M. Saliba, D. J. Hollman, S. D. Stranks, K. Wojciechowski, R. Avolio, G. Grancini, A. Petrozza, H. J. Snaith, *Nano Lett.* **2014**, *14*, 3247.

[97] X. Xiao, C. Bao, Y. Fang, J. Dai, B. R. Ecker, C. Wang, Y. Lin, S. Tang, Y. Liu, Y. Deng, X. Zheng, Y. Gao, X. C. Zeng, J. Huang, *Adv. Mater.* **2018**, *30*, 1705176.

[98] S. Lee, J. H. Park, B. R. Lee, E. D. Jung, J. C. Yu, D. Di Nuzzo, R. H. Friend, M. H. Song, *J. Phys. Chem. Lett.* **2017**, *8*, 1784.

[99] Y. Tian, A. Merdasa, M. Peter, M. Abdellah, K. Zheng, C. S. Ponseca, T. Pullerits, A. Yartsev, V. Sundström, I. G. Scheblykin, *Nano Lett.* **2015**, *15*, 1603.

[100] A. Swarnkar, R. Chulliyil, V. K. Ravi, M. Irfanullah, A. Chowdhury, A. Nag, *Angew. Chem., Int. Ed.* **2015**, *54*, 15424.

[101] D. W. Dequilettes, S. Koch, S. Burke, R. K. Paranji, A. J. Shropshire, M. E. Ziffer, D. S. Ginger, *ACS Energy Lett.* **2016**, *1*, 438.

[102] T. Y. Cheng, J. H. Lee, C. H. Chen, P. H. Chen, P. S. Wang, C. E. Lin, B. Y. Lin, Y. H. Lan, Y. H. Hsieh, J. J. Huang, H. F. Lu, I. Chao, M. kit Leung, T. L. Chiu, C. F. Lin, *Sci. Rep.* **2019**, *9*, 3654.

[103] Y. Liu, J. Cui, K. Du, H. Tian, Z. He, Q. Zhou, Z. Yang, Y. Deng, D. Chen, X. Zuo, Y. Ren, L. Wang, H. Zhu, B. Zhao, D. Di, J. Wang, R. H. Friend, Y. Jin, *Nat. Photonics* **2019**, *13*, 760.

[104] S. Kumar, J. Jagielski, N. Kallikounis, Y.-H. Kim, C. Wolf, F. Jenny, T. Tian, C. J. Hofer, Y.-C. Chiu, W. J. Stark, T.-W. Lee, C.-J. Shih, *Nano Lett.* **2017**, *17*, 5277.

[105] R. Wang, Y.-L. Jia, L. Ding, Z. He, Y. Dong, X.-J. Ma, Y. Zhang, D.-Y. Zhou, Z.-X. Zhu, Z.-H. Xiong, C.-H. Gao, *J. Appl. Phys.* **2019**, *126*, 165502.

[106] S. T. Ochsenbein, F. Krieg, Y. Shynkarenko, G. Rainò, M. V. Kovalenko, *ACS Appl. Mater. Interfaces* **2019**, *11*, 21655.

[107] F. Yang, H. Chen, R. Zhang, X. Liu, W. Zhang, J. Bin Zhang, F. Gao, L. Wang, *Adv. Funct. Mater.* **2020**, *30*, 1908760.

[108] F. Yan, J. Xing, G. Xing, L. Quan, S. T. Tan, J. Zhao, R. Su, L. Zhang, S. Chen, Y. Zhao, A. Huan, E. H. Sargent, Q. Xiong, H. V. Demir, *Nano Lett.* **2018**, *18*, 3157.

[109] J.-H. Lee, J.-J. Kim, *J. Inf. Disp.* **2013**, *14*, 39.

[110] B. Liu, L. Wang, H. Gu, H. Sun, H. V. Demir, *Adv. Opt. Mater.* **2018**, *6*, 1800220.

[111] Q. Shan, J. Li, J. Song, Y. Zou, L. Xu, J. Xue, Y. Dong, C. Huo, J. Chen, B. Han, H. Zeng, *J. Mater. Chem. C* **2017**, *5*, 4565.

[112] Z. Gao, Y. Zheng, Z. Wang, J. Yu, *J. Lumin.* **2018**, *201*, 359.

[113] R. Wang, Y. Zhang, F.-X. Yu, Y. Dong, Y.-L. Jia, X.-J. Ma, Q. Xu, Y. Deng, Z.-H. Xiong, C.-H. Gao, *J. Lumin.* **2020**, *219*, 116915.

[114] H. Shao, Y. Zhai, X. Wu, W. Xu, L. Xu, B. Dong, X. Bai, H. Cui, H. Song, *Nanoscale* **2020**, *12*, 11728.

[115] J. Jia, L. Zhu, Y. Wei, Z. Wu, H. Xu, D. Ding, R. Chen, D. Ma, W. Huang, *J. Mater. Chem. C* **2015**, *3*, 4890.

[116] L. S. Hung, C. W. Tang, M. G. Mason, *Appl. Phys. Lett.* **1997**, *70*, 152.

[117] C. I. Wu, G. R. Lee, T. W. Pi, *Appl. Phys. Lett.* **2005**, *87*, 212108.

[118] H. Heil, J. Steiger, S. Karg, M. Gastel, H. Ortner, H. Von Seggern, M. Stößel, *J. Appl. Phys.* **2001**, *89*, 420.

[119] G. L. Pakhomov, M. N. Drozdov, V. V. Travkin, M. N. Bochkarev, *Appl. Surf. Sci.* **2017**, *422*, 192.

[120] S. L Lai, M. Y Chan, M. K Fung, C. S Lee, L. S Hung, S. T Lee, *Chem. Phys. Lett.* **2002**, *366*, 128.

[121] M. U. Ali, J. Miao, J. Cai, D. F. Perepichka, H. Yang, H. Meng, *ACS Appl. Mater. Interfaces* **2020**, *12*, 18761.

[122] L. Qian, Y. Zheng, J. Xue, P. H. Holloway, *Nat. Photonics* **2011**, *5*, 543.

[123] Y.-H. Won, O. Cho, T. Kim, D.-Y. Chung, T. Kim, H. Chung, H. Jang, J. Lee, D. Kim, E. Jang, *Nature* **2019**, *575*, 634.

[124] K. Du, G. Liu, X. Chen, K. Wang, *J. Electrochem. Soc.* **2015**, *162*, E251.

[125] V. K. Ravi, G. B. Markad, A. Nag, *ACS Energy Lett.* **2016**, *1*, 665.

[126] Y. Wu, W. Chen, G. Chen, L. Liu, Z. He, R. Liu, *Nanomaterials* **2018**, *8*, 356.

[127] R. A. J. Janssen, J. W. Stouwdam, *J. Mater. Chem.* **2008**, *18*, 1889.

[128] X. Zhang, C. Sun, Y. Zhang, H. Wu, C. Ji, Y. Chuai, P. Wang, S. Wen, C. Zhang, W. W. Yu, *J. Phys. Chem. Lett.* **2016**, *7*, 4602.

[129] K. Qasim, B. Wang, Y. Zhang, P. Li, Y. Wang, S. Li, L. S. Tan, L. S. Liao, W. Lei, Q. Bao, *Adv. Funct. Mater.* **2017**, *27*, 1606874.

[130] L. Liu, Z. Wang, Z. Sun, W. Zhang, S. Hu, T. Hayat, A. Alsaedi, Z. Tan, *Chem. Commun.* **2018**, *54*, 13283.

[131] Z. Wang, F. Wang, W. Sun, R. Ni, S. Hu, J. Liu, B. Zhang, A. Alsaed, T. Hayat, Z. Tan, *Adv. Funct. Mater.* **2018**, *28*, 1804187.

[132] J. Pan, J. Chen, Q. Huang, Q. Khan, X. Liu, Z. Tao, Z. Zhang, W. Lei, A. Nathan, *ACS Photonics* **2016**, *3*, 215.

[133] J. Wang, C. Song, Z. He, C. Mai, G. Xie, L. Mu, Y. Cun, J. Li, J. Wang, J. Peng, Y. Cao, *Adv. Mater.* **2018**, *30*, 1804137.

[134] G. S. Kumar, B. Pradhan, T. Kamilya, S. Acharya, *Bull. Chem. Soc. Jpn.* **2018**, *91*, 1241.

[135] J. Wang, N. Wang, Y. Jin, J. Si, Z.-K. Tan, H. Du, L. Cheng, X. Dai, S. Bai, H. He, Z. Ye, M. L. Lai, R. H. Friend, W. Huang, *Adv. Mater.* **2015**, *27*, 2311.

[136] X. Zhao, Z.-K. Tan, *Nat. Photonics* **2020**, *14*, 215.

[137] L. Tang, J. Qiu, J. Wei, H. Gu, B. Du, H. Du, W. Hui, Y. Xia, Y. Chen, W. Huang, *ACS Appl. Mater. Interfaces* **2019**, *11*, 29132.

[138] Y.-H. Kim, T.-H. Han, H. Cho, S.-Y. Min, C.-L. Lee, T.-W. Lee, *Adv. Funct. Mater.* **2014**, *24*, 3808.

[139] G. Xing, N. Mathews, S. Sun, S. S. Lim, Y. M. Lam, M. Gratzel, S. Mhaisalkar, T. C. Sum, *Science* **2013**, *342*, 344.

[140] J. Li, Q. Yu, L. Gan, D. Chen, B. Lu, Z. Ye, H. He, *J. Mater. Chem. C* **2017**, *5*, 7715.

[141] Y. Zhan, X. Wang, G. Zhong, X. M. Ding, *Appl. Phys. Lett.* **2004**, *84*, 2913.

[142] Y. Shi, W. Wu, H. Dong, G. Li, K. Xi, G. Divitini, C. Ran, F. Yuan, M. Zhang, B. Jiao, X. Hou, Z. Wu, *Adv. Mater.* **2018**, *30*, 1800251.

[143] L. Zhang, F. Yuan, J. Xi, B. Jiao, H. Dong, J. Li, Z. Wu, *Adv. Funct. Mater.* **2020**, *30*, 2001834.

[144] H. Cho, Y.-H. Kim, C. Wolf, H.-D. Lee, T.-W. Lee, *Adv. Mater.* **2018**, *30*, 1704587.

[145] H. Kim, L. Zhao, J. S. Price, A. J. Grede, K. Roh, A. N. Brigeman, M. Lopez, B. P. Rand, N. C. Giebink, *Nat. Commun.* **2018**, *9*, 4893.

[146] Y. Zou, Z. Yuan, S. Bai, F. Gao, B. Sun, *Mater. Today Nano* **2019**, *5*, 100028.

[147] X. Zhang, W. Yin, W. Zheng, A. L. Rogach, *ACS Energy Lett.* **2020**, *5*, 2927.

**ADVANCED
SCIENCE NEWS**

www.advancedsciencenews.com

**ADVANCED
MATERIALS
INTERFACES**

www.advmatinterfaces.de

Eojin Yoon is studying for his Ph.D. course and received his B.S. degree in the Department of Materials Science and Engineering of Seoul National University. His current research includes organic–inorganic perovskite LED fabrication for displays based on multiple quantum well structure and lead-free perovskite LED fabrication.

Kyung Yeon Jang is studying for his Ph.D. course and received his B.S. degree in the Department of Materials Science and Engineering of Seoul National University. His current research focuses on synthesis of blue-emitting perovskite quantum dot and fabrication of perovskite LED for displays.

Jinwoo Park is studying for his Ph.D. course and received his B.S. degree in the Department of Materials Science and Engineering of Seoul National University. His current research interest includes synthesis of perovskite quantum dots and perovskite LED fabrication for displays.

Tae-Woo Lee is a full professor in materials science and engineering at the Seoul National University, Korea. He received his Ph.D. in chemical engineering from the Korea Advanced Institute of Science and Technology, Korea in 2002. He joined Bell Laboratories, USA as a postdoctoral researcher and worked Samsung Advanced Institute of Technology as a research staff (2003–2008). He was an associate professor in materials science and engineering at the Pohang University of Science and Technology (POSTECH), Korea until 2016. His research focuses on electronics based on organic and organic-inorganic hybrid materials for flexible displays, solid-state lightnings, and soler-energy-conversion devices.